RAD HRVATSKE AKADEMIJE ZNANOSTI I UMJETNOSTI
KNJIGA 521

HRVATSKA AKADEMIJA ZNANOSTI I UMJETNOSTI
RAZRED ZA TEHNIČKE ZNANOSTI

CROATIAN ACADEMY OF SCIENCES AND ARTS
DEPARTMENT OF TECHNCAL SCIENES

Razred za tehničke znanosti
Trg Nikole Šubića Zrinskog 11, Zagreb
vesvel@hazu.hr

Elektronička inačica svih tekstova objavljenih u časopisu dostupna je na središnjem portalu hrvatskih znanstvenih i stručnih časopisa HRČAK na e-adresi http: //hrcak.srce.hr/rtz. Urednik Aco Zrnić.

The electronic versions of all texts published in the journal are available on HRČAK, the central portal for Croatian scientific and expert journals. Link http: //hrcak.srce.hr/rtz. Editor Aco Zrnić.

UDK 62

ISSN 1848-8935 (Online)
ISSN 1330-0822 (Tisak)

R A D

HRVATSKE AKADEMIJE
ZNANOSTI I UMJETNOSTI

521

TEHNIČKE ZNANOSTI

17

ZAGREB, 2015.

CONTENTS / SADRŽAJ

Ivo Senjanović, Nikola Vladimir, Marko Tomić, Neven Hadžić
Timoshenko Beam Theory 93 Years Later – over Bridges to
Nanotubes and Ultra Large Ships 1
Sažetak: Timošenkova teorija grede nakon 93 godine – preko mostova do
nanocijevi i ultra velikih brodova 49
(Izvorni znanstveni članak / Original scientific paper)

Vatroslav V. Grubišić and Jani Barle
Procedure for the Service Strength Approval of the Drillship Derrick 51
Sažetak: Postupak provjere pogonske čvrstoce tornja broda za podmorska bušenja ... 63
(Izvorni znanstveni članak / Original scientific paper)

Srećko Sabalić, Janoš Kodvanj, Stjepan Jecić
The Position of the Implant for Extraarticular Fractures
of the Distal Humerus – the new Hypotheses for Management 65
Sažetak: Položaj implantata kod ekstraartikularnih prijeloma
distalnog humerusa – nove hipoteze za liječenje 76
(Pregledni članak / Rewiev article)

UDK / UDC 629.5
Izvorni znanstveni članak / Orginal scientific paper
Prihvaćeno / Accepted: 19. 2. 2015.

TIMOSHENKO BEAM THEORY 93 YEARS LATER – OVER BRIDGES TO NANOTUBES AND ULTRA LARGE SHIPS

Ivo Senjanović, Nikola Vladimir, Marko Tomić, Neven Hadžić

Abstract

An outline of the Timoshenko beam theory, which deals with deflection and cross-section rotation as the basic variables, is presented. It is modified by decomposing total deflection into pure bending deflection and shear deflection, and total rotation into bending rotation and axial shear angle. The governing equations are condensed into two independent equations of motion, one for flexural and another for axial shear vibrations. The solution is given for natural vibrations. Nonlocal stress parameter is taken into account for vibration analysis of nanotube embedded in an elastic medium. The 4^{th} order partial differential equation for flexural vibration is extended to the 6^{th} order one. Nanotube response to moving nanoparticle gravity load is analyzed by employing modal superposition method, separation of variables, Galerkin method and harmonic balance method. In addition coupled flexural and torsional vibrations of a thin-walled girder are considered. The modified Timoshenko beam theory is applied for flexural vibrations while the complex torsional beam theory with warping cross-section is worked out in an analogical way. For vibration analysis of nonprismatic ship hull an advanced beam finite element is created. Application of the developed theory is illustrated in the case of nanotube and ultra large container ship vibrations.

Keywords: Timoshenko beam theory; nanotube; moving load; thin-walled girder; flexural vibrations; torsional vibrations; container ship

Preface
Timoshenko's way from St. Petersburg to Stanford – via Zagreb
written by Stjepan Jecić

In engineering mechanical, especially supporting structures, the essential elements are the so-called girders. They are of different designs, and their basic geometrical

shapes are bars (beams), plates, walls, and shells, and variants thereof. In the first semesters of engineering studies, such as civil engineering, mechanical engineering and naval architecture, the strength of such elements is studied according to approximate theories adapted to the most common cases of actual structural designs. Thus, for instance, the calculation of beam elements is done according to the Euler-Bernoulli hypothesis which is valid for beams whose span l between the supports exceeds five heights h of the cross-section. Special cases are the beams on numerous mutually close supports with elastic characteristics and extreme cases of beams that rely on elastic bases. There are a lot of such cases known in engineering practice, such as railway tracks all the way to vessels – ships.

More accurate calculations of such special problems were the subject of research of scientists both of theoretical and applied mechanics at the end of the 19th century and further on intensively in all the years of the past twentieth century (e.g. E. Winkler, H. Zimmermann, W. Prager and others). Among these scientists special focus should be on a scientist theoretician, and above all pioneer of applied (engineering, technical) mechanics, Stephen Prokopovych Timoshenko. Born Ukrainian (in Shpotovka on 22 December 1878), he studied in St. Petersburg where he graduated in 1901 and acquired the university degree of an engineer of ways of communication. By starting to work at the Polytechnic Institute in St. Petersburg he acquired additional knowledge in theoretical mechanics under the supervision of very distinguished professor I.V. Mešćerski, and additional knowledge in mechanics of deformable bodies he acquired from the books and works of A. Föppel, whom he greatly admired. As a professor of mechanics he worked in Kiev (1906 – 1911) at the Faculty of Civil Engineering where he was also the Dean. From 1913, as professor of mechanics at the Polytechnics in St. Petersburg he held lectures and published a textbook on the Theory of Elasticity (1914). Scientifically he was dealing with problems of structural elements bending. He extended the Prandtl theory of boundary layer analogy to problems of torsion, and for the needs of shipbuilding of the Baltic fleet he developed procedures of calculating stability of stiffened panels. It is interesting to mention that at that time Timoshenko defined and determined the so-called shear centre for beams in which the resulting load does not pass through the centre of gravity of the girder cross-section. At the beginning of the First World War he published his original idea, observing the railway tracks as girders on an elastic bedding. He published a paper dealing with this topic in the Works of the St. Petersburg Ways of Communication Institute.

In the whirlwind of war and political events the life and work in St. Petersburg were becoming increasingly difficult. Timoshenko took refuge with his family in a relatively peaceful Kiev. However, war and revolutionary developments forced Ste-

phen Timoshenko to move with quite a large group of refugees towards Sevastopol where, together with his former student J.M. Hlitčijev, he decided to move to Serbia. Passing across Turkey, after several weeks of toilsome travelling they arrived in Belgrade. The city was full of refugees and it was impossible to find any accommodation. After a short time, the Belgrade professor of mechanics Arnovljević found him accommodation at his sister's place in Zemun. Realizing that in 1919 the Technical Higher School was to be founded in Zagreb, he sent his job application and was admitted as the professor of Science of Strength of Materials starting in April 1920. He stayed in Zagreb until the end of the academic year 1922 where he established a Department for technical mechanics. However, his junior colleague Hlitčijev, a shipbuilding engineer, remained all his life in Belgrade as a distinguished university professor and member of the Serbian Academy of Sciences.

Although Stephen Timoshenko describes Zagreb as a city of pro-European appearance and culture, his life in this city was not comfortable. Zagreb could not offer any appropriate accommodation, so by the approval of the Rector he was placed with his family in the premises of the future laboratory for material testing. On improvised furniture the whole family lived for two years modestly and in a cramped space, which resulted in Timoshenko's decision in 1922 to move to the United States. Yet, even in such circumstances he was active scientifically, and retreated from undesirable visitors to the university library into peace and quiet.

Still while he was staying in Zemun, he used the time to develop arithmetic procedures of solving various problems important in shipbuilding. The continuation of intensive work in Zagreb brought to two major publications in the field of transversal vibrations of beams abandoning the Euler-Bernoulli hypothesis. It is, namely, in bending of short beams that the cross-sections deflect more from their original position and do not stay perpendicular to the neutral axis of the girder, and therefore the application of a simple theory of bending will lead to the wrong result greater than 1%. With the paper *On the correction for shear of the differential equation for transverse vibration of prismatic bars* and the paper *On the transverse vibrations of bars of uniform cross section* Timoshenko solved the problem in a way applicable to the engineering practice, although solving finite equations satisfying the given boundary conditions was a demanding job. Both papers were published in 1921 and 1922 in the Journal *Philosophical Magazine*, and in this Timoshenko received great help from the English mathematician E.H. Love, one of the founders of mathematical theory of elasticity. Today's powerful computers provide almost unlimited possibilities for the application of direct methods of searching for solutions numerically (e.g. finite difference method). However, new numerical methods, developed from the middle of the past

century provide a better and more convenient tool. Among them, the method of finite elements is definitely unmatched. Today in literature the usual term for such problems related to the beams is *Timoshenko beam theory*.

In Zagreb Stephen Timoshenko has been remembered as an excellent scientist, and foremost as an excellent lecturer, delivering lectures initially in Russian, and later, with the help of an assistant in the Croatian language. He left Zagreb in the summer of 1922 moving with his family first to Philadelphia and then to Pittsburgh. In 1927 he became Professor at the University of Michigan. From 1936 until his retirement he was Professor of mechanics at the Stanford University. On several occasions he visited Europe. On two occasions, in 1958 and 1967, Timoshenko visited Kiev, which was described in more detail by the Kiev academician G.S. Pisarenko who was his host and wrote the afterword to the second edition of Timoshenko's book *Vospominanija*. In 1956 Timoshenko received a honorary doctorate of science of the University of Zagreb. On that occasion he visited the Faculty of Engineering, writing about it with words of praise in his *Memoirs* describing the huge progress and development from the time of his work in Zagreb. In Switzerland in 1964 he had the bad luck of breaking his leg and that same autumn his elder daughter Ana escorted him in a wheelchair to the opening of the International Congress of Mechanics in Munich. Timoshenko was greeted with a round of applause receiving thus tribute from more than 1,000 attendees as one of the greatest mechanical engineers of that time. Unable to return to the USA he remained until the end of his life (29 May 1972) with his daughter Ana in Wuppertal. His urn was laid next to his wife in Palo Alto in California.

1. INTRODUCTION

Beam is used as a structural element in many engineering structures like frame and grillage ones, [1,2,3]. Also, the whole complex structures like bridges, ship hulls, floating airports, etc. can be modeled as a beam. Hence, instead of 3D FEM model, beam model is used with cross-section properties determined as equivalent quantities of 2D sectional structure. In case of structure with large aspect ratio of height and length the Timoshenko beam theory is used, instead of the Euler-Bernoulli theory, since it takes both shear and rotary inertia into account. Their influence is especially pronounced in higher natural modes.

The Timoshenko beam theory was published 93 years ago, and during that long time it has been successfully used for static and dynamic analysis of any type of beam-like structures, [4,5]. That theory deals with two differential equations of motion with deflection and cross-section rotation as the basic variables. The system is reduced into a single the 4^{th} order partial differential equation by Timoshenko [6], where only an

approximate solution is given as commented in [7,8]. Almost in all papers the first approach with two differential equations is used in order to ensure control of exact and complete beam behavior, [8,9].

The Timoshenko beam theory is applied also for more complex problems as for instance beam vibrations on elastic foundation, [10], beam vibrations and buckling on elastic foundation, [11], vibrations of double-beam system with transverse and axial load, [12], vibration and stability of multiple beam systems, [13], beam response due to moving gravity and inertia load related to railway and highway bridges, [14-17], etc. Recent decades the Timoshenko beam theory is used in nanotechnology for vibration analysis of nanotubes exposed to moving nanoparticle load, [18-21].

Timoshenko's idea of shear and rotary inertia influence on deflection is not only limited to beams. These effects are also incorporated into the Mindlin thick plate theory as well as into its modification, as 2D problem, [22,23]. Timoshenko beam static deflection functions are often used as coordinate functions for thick plate vibration analysis by the Rayleigh-Ritz method, [24]. Furthermore, differential equation of beam torsion with shear influence is based on analogy with that for beam bending, [25]. Hence, in case of coupled flexural and torsional vibrations of a girder with open cross-section the same mathematical model is used for analysis of both responses.

The Timoshenko beam theory plays an important role in development of sophisticated beam finite element. Various finite elements have been worked out in the last decades. They are distinguished into the choice of interpolation functions for mathematical description of beam deflection and cross-section rotation. Application of the same order polynomials for both displacements leads to the so-called shear locking problem, since bending strain energy for a slender beam vanishes before shear strain energy. If static solution of Timoshenko beam is used for deflection and rotation functions the problem is overcome, [26].

In spite of the fact that enormous number of papers has been published by employing Timoshenko beam theory from 1922, it seems that all phenomena hidden in that theory are not yet investigated. For instance problem of beam response due to moving gravity and inertia force related to bridges is analyzed in literature in different ways. Presently, a systematic investigation of that problem is undertaken in [27] in order to establish the simplest mathematical formulation. Hence, original and modified Timoshenko beam theory is used in combination with Galerkin method and energy balance. The problem is solved completely in analytical way employing the perturbation method.

Motivated by the above described state-of-the art in this article modified Timoshenko beam theory, with bending deflection as the single based variable, and its advantages are presented, [28]. It is applied for nanotube vibrations due to moving

nanoparticle load, [29], by employing results from [26]. Also, an advanced beam finite element for coupled flexural and torsional vibration analysis of thin-walled girder is worked out. Its application is illustrated in case of an ultra large container ship, [30].

2. OUTLINE OF THE TIMOSHENKO BEAM THEORY

Timoshenko beam theory deals with beam deflection and angle of rotation of cross-section, w and ψ, respectively, [4,5]. The sectional forces, i.e. bending moment and shear force read

$$M = D\frac{\partial \psi}{\partial x}, \qquad Q = S\left(\frac{\partial w}{\partial x} + \psi\right), \tag{1}$$

where *D=EI* is flexural rigidity and $S = k_S GA$ is shear rigidity, *A* is cross-section area and *I* is its moment of inertia, k_S is shear coefficient, and *E* and $G = E/\left(2\left(1+\nu\right)\right)$ is Young's modulus and shear modulus, respectively. Value of shear coefficient depends on beam cross-section profile, [31].

Beam is loaded with transverse inertia load per unit length, and distributed bending moment

$$q_x = -m\frac{\partial^2 w}{\partial t^2}, \qquad m_x = -J\frac{\partial^2 \psi}{\partial t^2}, \tag{2}$$

where $m = \rho A$ is specific mass and $J = \rho I$ is mass moment of inertia, both per unit length.

Equilibrium of moments and forces

$$\frac{\partial M}{\partial x} - Q = -m_x, \qquad \frac{\partial Q}{\partial x} = -q_x \tag{3}$$

leads to two coupled differential equations

$$D\frac{\partial^2 \psi}{\partial x^2} - S\left(\frac{\partial w}{\partial x} + \psi\right) - J\frac{\partial^2 \psi}{\partial t^2} = 0 \tag{4}$$

$$S\left(\frac{\partial^2 w}{\partial x^2} + \frac{\partial \psi}{\partial x}\right) - m\frac{\partial^2 w}{\partial t^2} = 0\,. \tag{5}$$

From (5) yields

$$\frac{\partial \psi}{\partial x} = -\frac{\partial^2 w}{\partial x^2} + \frac{m}{S}\frac{\partial^2 w}{\partial t^2} \tag{6}$$

and by substituting (6) into (4) derived per x, one arrives at the single beam differential equation of motion

$$\frac{\partial^4 w}{\partial x^4} - \left(\frac{J}{D} + \frac{m}{S} \right) \frac{\partial^4 w}{\partial x^2 \partial t^2} + \frac{m}{D} \frac{\partial^2}{\partial t^2} \left(w + \frac{J}{S} \frac{\partial^2 w}{\partial t^2} \right) = 0 . \tag{7}$$

Once (7) is solved angle of rotation is obtained from (6) as

$$\psi = -\frac{\partial w}{\partial x} + \frac{m}{S} \int \frac{\partial^2 w}{\partial t^2} \mathrm{d}x + f(t) , \tag{8}$$

where $f(t)$ is rigid body motion.

3. MODIFIED TIMOSHENKO BEAM THEORY

3.1 Differential equations of motion

In order to make the beam theory more physically transparent, beam deflection w and angle of rotation ψ are split into their constitutive parts, [28], Fig. 1, i.e.

$$w = w_b + w_s , \qquad \psi = \varphi + \vartheta , \qquad \varphi = -\frac{\partial w_b}{\partial x} , \tag{9}$$

where w_b and w_s is beam deflection due to pure bending and transverse shear, respectively, and φ is angle of cross-section rotation due to bending, while ϑ is cross-section slope due to axial shear. Newly introduced phenomenology as well as additional explanations are thoroughly presented in [28]. Equilibrium equations (4) and (5) can be presented in the form with the separated variables w_b and w_s, and ϑ

$$D \frac{\partial^3 w_b}{\partial x^3} - J \frac{\partial^2}{\partial t^2} \left(\frac{\partial w_b}{\partial x} \right) + S \frac{\partial w_s}{\partial x} = D \frac{\partial^2 \vartheta}{\partial x^2} - S\vartheta - J \frac{\partial^2 \vartheta}{\partial t^2} \tag{10}$$

$$S \frac{\partial^2 w_s}{\partial x^2} - m \frac{\partial^2}{\partial t^2} \left(w_b + w_s \right) = -S \frac{\partial \vartheta}{\partial x} . \tag{11}$$

Since only two equations are available for three variables one can assume that flexural shear, w_s, and slope due to axial shear, ϑ, are not coupled. In that case, by setting both left and right hand side of (10) zero, yields from the former

$$w_s = -\frac{D}{S} \frac{\partial^2 w_b}{\partial x^2} + \frac{J}{S} \frac{\partial^2 w_b}{\partial t^2} . \tag{12}$$

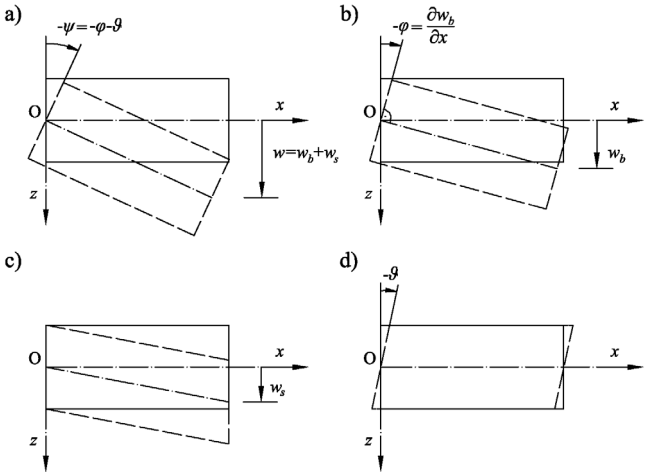

Fig. 1. Thick beam displacements; a – total deflection and rotation w,ψ , b – pure bending deflection and rotation w_b,φ , c – transverse shear deflection w_s , d – axial shear angle ϑ

Sl. 1. Pomaci debele grede: a – ukupni progib i kut zakreta w,ψ , b – progib čistog savijanja i kut zakreta w_b,φ , c – progib poprečnog smicanja w_s , d – kut uzdužnog smicanja ϑ

By substituting (12) into (11) differential equation for flexural vibrations is obtained, which is expressed with pure bending deflection

$$\frac{\partial^4 w_b}{\partial x^4}-\left(\frac{J}{D}+\frac{m}{S}\right)\frac{\partial^4 w_b}{\partial x^2\partial t^2}+\frac{m}{D}\frac{\partial^2}{\partial t^2}\left(w_b+\frac{J}{S}\frac{\partial^2 w_b}{\partial t^2}\right)=\frac{S}{D}\frac{\partial\vartheta}{\partial x} \tag{13}$$

Disturbing function on the right hand side in (13) can be ignored due to assumed uncoupling of flexural and axial shear vibrations. Once w_b is determined, the total beam deflection, according to (9), reads

$$w=w_b-\frac{D}{S}\frac{\partial^2 w_b}{\partial x^2}+\frac{J}{S}\frac{\partial^2 w_b}{\partial t^2}. \tag{14}$$

The right hand side of (10) represents differential equation of axial shear vibrations

$$\frac{\partial^2\vartheta}{\partial x^2}-\frac{S}{D}\vartheta-\frac{J}{D}\frac{\partial^2\vartheta}{\partial t^2}=0, \tag{15}$$

as given in [28].

3.2 General solution of flexural vibrations

Natural vibrations are harmonic, i.e. $w_b = W_b \sin \omega t$ and $\vartheta = \Theta \sin \omega t$, so that equations of motion (13) and (15) are related to the vibration amplitudes

$$\frac{\mathrm{d}^4 W_b}{\mathrm{d}x^4} + \omega^2 \left(\frac{J}{D} + \frac{m}{S} \right) \frac{\mathrm{d}^2 W_b}{\mathrm{d}x^2} + \omega^2 \frac{m}{D} \left(\omega^2 \frac{J}{S} - 1 \right) W_b = 0 \tag{16}$$

$$\frac{\mathrm{d}^2 \Theta}{\mathrm{d}x^2} + \frac{S}{D} \left(\omega^2 \frac{J}{S} - 1 \right) \Theta = 0 . \tag{17}$$

Amplitude of total deflection, according to (14), reads

$$W = \left(1 - \omega^2 \frac{J}{S} \right) W_b - \frac{D}{S} \frac{\mathrm{d}^2 W_b}{\mathrm{d}x^2} . \tag{18}$$

Eq. (16) is known in literature as a reliable alternative of Timoshenko differential equations, [32,33].

Solution of (16) can be assumed in the form $W_b = A e^{\gamma x}$ that leads to biquadratic equation

$$\gamma^4 + a\gamma^2 + b = 0 , \tag{19}$$

where

$$a = \omega^2 \left(\frac{J}{D} + \frac{m}{S} \right), \qquad b = \omega^2 \frac{m}{D} \left(\omega^2 \frac{J}{S} - 1 \right). \tag{20}$$

Roots of (19) read

$$\gamma = \alpha, -\alpha, i\beta, -i\beta , \tag{21}$$

where $i = \sqrt{-1}$ and

$$\begin{aligned} \alpha &= \frac{\omega}{\sqrt{2}} \sqrt{\sqrt{\left(\frac{m}{S} - \frac{J}{D} \right)^2 + \frac{4m}{D\omega^2}} - \left(\frac{m}{S} + \frac{J}{D} \right)}, \\ \beta &= \frac{\omega}{\sqrt{2}} \sqrt{\sqrt{\left(\frac{m}{S} - \frac{J}{D} \right)^2 + \frac{4m}{D\omega^2}} + \left(\frac{m}{S} + \frac{J}{D} \right)}. \end{aligned} \tag{22}$$

Hence, solution of Eq. (16) is obtained in the form

$$W_b = A_1 \sinh \alpha x + A_2 \cosh \alpha x + A_3 \sin \beta x + A_4 \cos \beta x . \tag{23}$$

By employing expressions for displacements and forces one arrives at

$$W = A_1\left(1-\omega^2\frac{J}{S}-\alpha^2\frac{D}{S}\right)\mathrm{sh}\alpha x + A_2\left(1-\omega^2\frac{J}{S}-\alpha^2\frac{D}{S}\right)\mathrm{ch}\alpha x$$
$$+ A_3\left(1-\omega^2\frac{J}{S}+\beta^2\frac{D}{S}\right)\sin\beta x + A_4\left(1-\omega^2\frac{J}{S}+\beta^2\frac{D}{S}\right)\cos\beta x$$
$$\Phi = -\frac{\mathrm{d}W_b}{\mathrm{d}x} = -\left(A_1\alpha\,\mathrm{ch}\alpha x + A_2\alpha\,\mathrm{sh}\alpha x + A_3\beta\cos\beta x - A_4\beta\sin\beta x\right) \tag{24}$$
$$M = -D\frac{\mathrm{d}^2W_b}{\mathrm{d}x^2} = -D\left(A_1\alpha^2\mathrm{sh}\alpha x + A_2\alpha^2\mathrm{ch}\alpha x - A_3\beta^2\sin\beta x - A_4\beta^2\cos\beta x\right)$$

$$Q = -D\frac{\mathrm{d}^3W_b}{\mathrm{d}x^3} - \omega^2 J\frac{\mathrm{d}W_b}{\mathrm{d}x} = -D\left[A_1\alpha\left(\alpha^2+\omega^2\frac{J}{D}\right)\mathrm{ch}\alpha x + A_2\alpha\left(\alpha^2+\omega^2\frac{J}{D}\right)\mathrm{sh}\alpha x - \right.$$
$$\left. - A_3\beta\left(\beta^2-\omega^2\frac{J}{D}\right)\cos\beta x + A_4\beta\left(\beta^2-\omega^2\frac{J}{D}\right)\sin\beta x\right].$$

3.3 General solution of axial shear vibrations

Differential equations (17) for natural axial shear vibrations of beam reads

$$\frac{\mathrm{d}^2\Theta}{\mathrm{d}x^2} + \left(\omega^2\frac{J}{D}-\frac{S}{D}\right)\Theta = 0\,. \tag{25}$$

It is similar to the equation for rod stretching vibrations

$$\frac{\mathrm{d}^2u}{\mathrm{d}x^2} + \omega_R^2\frac{m}{EA}u = 0\,. \tag{26}$$

The difference is the additional moment $S\Theta$, which is associated to inertia moment $\omega^2 J\Theta$, and represents reaction of an imagined rotational elastic foundation with stiffness equal to the shear stiffness *S*, as shown in Fig. 2.

Solution of (26) and corresponding axial force $N = EA\dfrac{\mathrm{d}u}{\mathrm{d}x}$ read

$$u = C_1\sin\chi x + C_2\cos\chi x,$$
$$N = EA\left(C_1\chi\cos\chi x - C_2\chi\sin\chi x\right), \tag{27}$$

where $\chi = \omega_R\sqrt{m/(EA)}$. Based on analogy between (25) and (26) one can write for shear slope angle and moment

$$\begin{aligned} \Theta &= C_1 \sin \eta x + C_2 \cos \eta x, \\ M &= D\left(C_1 \eta \cos \eta x - C_2 \eta \sin \eta x\right) \end{aligned} \tag{28}$$

where

$$\eta = \sqrt{\omega^2 \frac{J}{D} - \frac{S}{D}} \,. \tag{29}$$

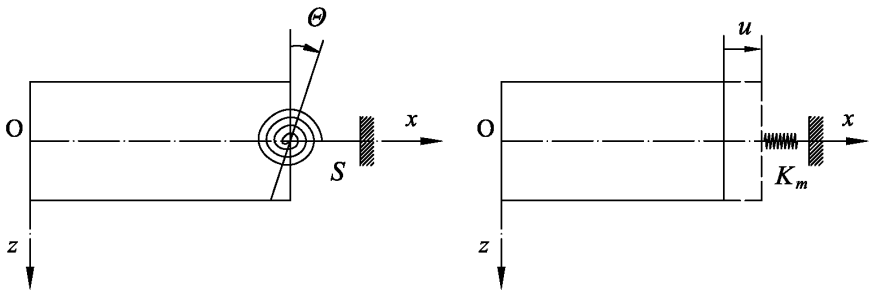

Fig. 2. Analogy between axial shear model and stretching model

Sl. 2. Analogija između modela uzdužnog smicanja i rastezanja

4. NONLOCAL VIBRATIONS OF A CARBON NANOTUBE DUE TO MOVING NANOPARTICLE GRAVITY FORCE

4.1 Differential equation of nonlocal vibrations

In the modified Timoshenko beam theory the basic variable is bending deflection w_b, so the total deflection reads $w = w_b + w_s$, where w_s is shear deflection (12). Nonlocal effect is included in the definition of beam bending moment and shear force of nanotube according to [18]

$$M - \mu \frac{\partial^2 M}{\partial x^2} = -D \frac{\partial^2 w_b}{\partial x^2}, \tag{30}$$

$$Q - \mu \frac{\partial^2 Q}{\partial x^2} = -D \frac{\partial^3 w_b}{\partial x^3} + J \frac{\partial^3 w_b}{\partial x \partial t^2}, \tag{31}$$

where $\mu = (e_0 a)^2$ is nonlocal parameter related to the second stress gradient, e_0 is a constant and a is an internal characteristic length, [18]. Dynamic equilibrium of bending moments and transverse forces acting on beam differential element reads, Fig. 3,

$$\frac{\partial M}{\partial x} - Q = -J\frac{\partial^3 w_b}{\partial x \partial t^2}, \tag{32}$$

$$\frac{\partial Q}{\partial x} = k_w w + m\frac{\partial^2 w}{\partial t^2} - q, \tag{33}$$

where k_w is stiffness of elastic support, $m = \rho A$ is mass per unit length, A is cross-section area, and q is distributed external excitation. By eliminating Q from (32) by (33) yields

$$\frac{\partial^2 M}{\partial x^2} = k_w w + m\frac{\partial^2 w}{\partial t^2} - J\frac{\partial^4 w_b}{\partial x^2 \partial t^2} - q, \tag{34}$$

while (33) can be written in the form

$$\frac{\partial^2 Q}{\partial x^2} = k_w \frac{\partial w}{\partial x} + m\frac{\partial^3 w}{\partial x \partial t^2} - \frac{\partial q}{\partial x}. \tag{35}$$

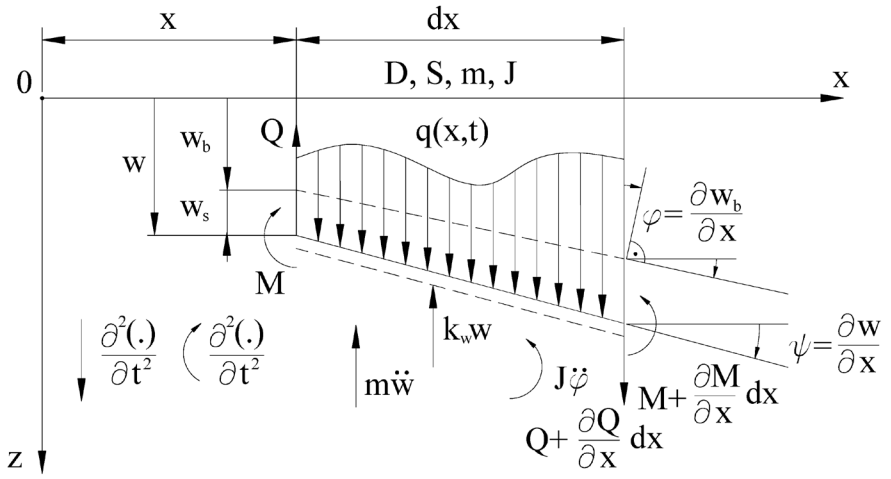

***Fig.* 3.** Displacements and forces on differential element of a beam on elastic foundation

***Sl.* 3.** Pomaci i sile na diferencijalnom elementu grede na elastičnoj podlozi

Substituting (34) and (35) into (30) and (31) respectively, one arrives at

$$M = -D\frac{\partial^2 w_b}{\partial x^2} + \mu\left(k_w w + m\frac{\partial^2 w}{\partial t^2} - J\frac{\partial^4 w_b}{\partial x^2 \partial t^2} - q \right), \tag{36}$$

$$Q = -D\frac{\partial^3 w_b}{\partial x^3} + J\frac{\partial^3 w_b}{\partial x \partial t^2} + \mu\left(k_w \frac{\partial w}{\partial x} + m\frac{\partial^3 w}{\partial x \partial t^2} - \frac{\partial q}{\partial x} \right). \tag{37}$$

Furthermore, inserting (37) into (33), equilibrium equation with nonlocal effect in terms of w and w_b is obtained

$$D\frac{\partial^4 w_b}{\partial x^4} - J\frac{\partial^4 w_b}{\partial x^2 \partial t^2} + m\frac{\partial^2 w}{\partial t^2} + k_w w - \mu\left(m\frac{\partial^4 w}{\partial x^2 \partial t^2} + k_w \frac{\partial^2 w}{\partial x^2} \right) = q - \mu\frac{\partial^2 q}{\partial x^2}. \tag{38}$$

Referring to (9) and (12), total deflection reads

$$w = w_b - \frac{D}{S}\frac{\partial^2 w_b}{\partial x^2} + \frac{J}{S}\frac{\partial^2 w_b}{\partial t^2}, \tag{39}$$

and substituting (39) into (38) partial differential equation of vibrations in terms of single variable w_b is obtained

$$\begin{aligned} &\mu\frac{m}{S}\frac{\partial^6 w_b}{\partial x^4 \partial t^2} - \mu\frac{mJ}{DS}\frac{\partial^6 w_b}{\partial x^2 \partial t^4} + \left(1 + \mu\frac{k_w}{S}\right)\frac{\partial^4 w_b}{\partial x^4} \\ &\quad - \frac{m}{S}\left[1 + \frac{SJ}{Dm} + \mu\frac{S}{D}\left(1 + \frac{k_w J}{Sm}\right)\right]\frac{\partial^4 w_b}{\partial x^2 \partial t^2} + \frac{mJ}{DS}\frac{\partial^4 w_b}{\partial t^4} \\ &\quad - \frac{k_w}{S}\left(1 + \mu\frac{S}{D}\right)\frac{\partial^2 w_b}{\partial x^2} + \frac{m}{D}\left(1 + \frac{k_w J}{Sm}\right)\frac{\partial^2 w_b}{\partial t^2} + \frac{k_w}{D} w_b = \frac{q}{D} - \frac{\mu}{D}\frac{\partial^2 q}{\partial x^2}. \end{aligned} \tag{40}$$

The equation (40) is of the sixth order, i.e. the fourth order per x and t. If $\mu = 0$ and $k_w = 0$ Eq. (40) is reduced to the modified Timoshenko equation, [28].

4.2 Natural vibrations

Natural vibrations are harmonic functions $w_b(x,t) = W_b(x)\sin\omega t$, where w_b is bending natural mode and ω is natural frequency. Now Eq. (40) is reduced to w_b, which depends on ω, and can be presented in the form

$$a\frac{\mathrm{d}^4W_b}{\mathrm{d}x^4}+b\frac{\mathrm{d}^2W_b}{\mathrm{d}x^2}+cW_b=0, \tag{41}$$

where

$$a=1+\mu\frac{k_w}{S}-\omega^2\mu\frac{m}{S},$$

$$b=-\frac{k_w}{S}\left(1+\mu\frac{S}{D}\right)+\omega^2\frac{m}{S}\left[1+\frac{SJ}{Dm}+\mu\frac{S}{D}\left(1+\frac{k_wJ}{Sm}\right)\right]-\omega^4\mu\frac{mJ}{DS}, \tag{42}$$

$$c=\frac{k_w}{D}-\omega^2\frac{m}{D}\left(1+\frac{k_wJ}{Sm}\right)+\omega^4\frac{mJ}{DS}.$$

Solution of (41) is assumed in exponential form $W_b=Ae^{\gamma x}$ that leads to biquadratic characteristic equation

$$a\gamma^4+b\gamma^2+c=0. \tag{43}$$

with roots

$$\gamma_{1,2}=\pm\alpha,\ \gamma_{3,4}=\pm i\beta, \tag{44}$$

where

$$\alpha,\beta=\frac{1}{\sqrt{2a}}\sqrt{\sqrt{b^2-4ac}\mp b}. \tag{45}$$

Bending deflection is obtained in the form (23) and displacements and sectional forces, according to (18), (36) and (37) respectively, read

$$W=\left(1-\omega^2\frac{J}{S}\right)W_b-\frac{D}{S}\frac{\mathrm{d}^2W_b}{\mathrm{d}x^2}$$
$$=A_1a_1\sinh\alpha x+A_2a_1\cosh\alpha x+A_3a_2\sin\beta x+A_4a_2\cos\beta x,$$

$$\Phi=\frac{\mathrm{d}W_b}{\mathrm{d}x}=A_1\alpha\cosh\alpha x+A_2\alpha\sinh\alpha x+A_3\beta\cos\beta x-A_4\beta\sin\beta x,$$

$$M_x=-b_1\frac{\mathrm{d}^2W_b}{\mathrm{d}x^2}+b_2W_b \tag{46}$$
$$=A_1\left(-b_1\alpha^2+b_2\right)\sinh\alpha x+A_2\left(-b_1\alpha^2+b_2\right)\cosh\alpha x$$
$$+A_3\left(b_1\beta^2+b_2\right)\sin\beta x+A_4\left(b_1\beta^2+b_2\right)\cos\beta x,$$

$$
\begin{aligned}
Q_x &= -c_1 \frac{\mathrm{d}^3 W_b}{\mathrm{d}x^3} + c_2 \frac{\mathrm{d}W_b}{\mathrm{d}x} \\
&= A_1 \left(-c_1\alpha^2 + c_2\right)\alpha \cosh \alpha x + A_2 \left(-c_1\alpha^2 + c_2\right)\alpha \sinh \alpha x \\
&\quad + A_3 \left(c_1\beta^2 + c_2\right)\beta \cos \beta x - A_4 \left(c_1\beta^2 + c_2\right)\beta \sin \beta x,
\end{aligned}
$$

where

$$
\begin{aligned}
&a_1 = 1 - \omega^2 \frac{J}{S} - \alpha^2 \frac{D}{S},\ a_2 = 1 - \omega^2 \frac{J}{S} + \beta^2 \frac{D}{S}, \\
&b_1 = D + \mu \left[k_w \frac{D}{S} - \omega^2 J \left(1 + \frac{Dm}{SJ} \right) \right],\ b_2 = \mu \left(k_w - \omega^2 m \right) \left(1 - \omega^2 \frac{J}{S} \right), \\
&c_1 = D + \mu \left(k_w - \omega^2 m \right) \frac{D}{S},\ c_2 = -\omega^2 J + \mu \left(k_w - \omega^2 m \right) \left(1 - \omega^2 \frac{J}{S} \right).
\end{aligned} \tag{47}
$$

Integration constants A_k, $\mathrm{k} = 1,2,3,4$, are determined by satisfying boundary conditions. Simply supported beam is a special case since boundary conditions $W(0) = W(l) = 0$ and $M_x(0) = M_x(l) = 0$ are satisfied by trigonometric function $W_b = \sin \frac{i\pi x}{l}$. Substituting W_b into differential equation (41), and grouping terms of the same power of ω, the frequency equation is obtained

$$
\tilde{a}\omega^4 - \tilde{b}\omega^2 + \tilde{c} = 0, \tag{48}
$$

where

$$
\begin{aligned}
&\tilde{a} = \frac{mJ}{DS} \left[1 + \mu \left(\frac{i\pi}{l} \right)^2 \right], \\
&\tilde{b} = \frac{m}{D} \left(1 + \frac{k_w J}{Sm} \right) + \frac{m}{S} \left[1 + \frac{SJ}{Dm} + \mu \frac{S}{D} \left(1 + \frac{k_w J}{Sm} \right) \right] \left(\frac{i\pi}{l} \right)^2 + \mu \frac{m}{S} \left(\frac{i\pi}{l} \right)^4, \\
&\tilde{c} = \frac{k_w}{D} + \frac{k_w}{S} \left(1 + \mu \frac{S}{D} \right) \left(\frac{i\pi}{l} \right)^2 + \left(1 + \mu \frac{k_w}{S} \right) \left(\frac{i\pi}{l} \right)^4.
\end{aligned} \tag{49}
$$

Solutions of Eq. (48) read

$$
\omega_{1,2} = \frac{1}{\sqrt{2\tilde{a}}} \sqrt{\tilde{b} \pm \sqrt{\tilde{b}^2 - 4\tilde{a}\tilde{c}}}\,. \tag{50}
$$

It is obvious that two frequency spectra are obtained as a characteristic of simply supported beam. They are shifted for

$$\omega_1^2 - \omega_2^2 = \frac{1}{\tilde{a}}\sqrt{\tilde{b}^2 - 4\tilde{a}\tilde{c}}. \tag{51}$$

4.3 Forced vibrations due to moving gravity force

Vibrations of a simply supported single-walled carbon nanotube (SWCNT), embedded in elastic medium and excited by weight of moving nanoparticle, are analyzed, Fig. 4. Modal superposition method and separation of variables approach are used for solving governing partial differential equation (40). Accordingly, bending deflection is assumed in the form

$$w_b(x,t) = \sum_{j=1}^{\infty} W_{bj}(x)\, T_j(t), \tag{52}$$

where $W_{bj}(x)$ is natural mode and $T_j(t)$ is unknown time dependent function. Eq. (52) is substituted into (40), and applying the Galerkin method, it is further multiplied with mode function $W_{bi}(x)$ and integrated over the beam length. As a result, the following modal equation in terms of generalized displacements is obtained

$$\begin{aligned}
&\sum_{j=1}^{\infty} \frac{mJ}{DS}\left(I_{ij}^{(0)} - \mu I_{ij}^{(2)}\right)\dddot{T}_j \\
&+\sum_{j=1}^{\infty}\left\{\mu\frac{m}{S}I_{ij}^{(4)} - \frac{m}{S}\left[1+\frac{SJ}{Dm}+\mu\frac{S}{D}\left(1+\frac{k_w J}{Sm}\right)\right]I_{ij}^{(2)} + \frac{m}{D}\left(1+\frac{k_w J}{Sm}\right)I_{ij}^{(0)}\right\}\ddot{T}_j \\
&+\sum_{j=1}^{\infty}\left[\left(1+\mu\frac{k_w}{S}\right)I_{ij}^{(4)} - \frac{k_w}{S}\left(1+\mu\frac{S}{D}\right)I_{ij}^{(2)} + \frac{k_w}{D}I_{ij}^{(0)}\right]T_j = \frac{1}{D}\int_0^l\left(q - \mu\frac{\partial^2 q}{\partial x^2}\right)W_{bi}\,\mathrm{d}x,
\end{aligned} \tag{53}$$

where $i = 1, 2, \ldots$ and

$$I_{ij}^{(0)} = \int_0^l W_{bi}W_{bj}\,\mathrm{d}x,\ I_{ij}^{(2)} = \int_0^l W_{bi}W_{bj}''\,\mathrm{d}x,\ I_{ij}^{(4)} = \int_0^l W_{bi}W_{bj}''''\,\mathrm{d}x. \tag{54}$$

The above system of ordinary linear differential equations of the fourth order can be written in matrix notation

$$\left[N_{ij}\right]\left\{\dddot{T}_j\right\} + \left[M_{ij}\right]\left\{\ddot{T}_j\right\} + \left[K_{ij}\right]\left\{T_j\right\} = \left\{F_i\right\}, \tag{55}$$

where

$$F_i = \frac{1}{D}\int_0^l \left(q - \mu \frac{\partial^2 q}{\partial x^2} \right) W_{bi} \mathrm{d}x \tag{56}$$

is the generalized excitation force. In the considered case one is faced with constant lumped nanoparticle gravity force, P, Fig. 4. Using partial integration

$\int_0^l \frac{\partial^2 q}{\partial x^2} \mathrm{W}_{bi} \mathrm{d}x = \int_0^l q \frac{\partial^2 \mathrm{W}_{bi}}{\partial x^2} \mathrm{d}x$ and $q = P/\mathrm{d}x$ one obtains

$$F_i = \frac{P}{D}\left[W_{bi}(x_P) - \mu W''_{bi}(x_P) \right], \tag{57}$$

where the force position is linearly changed due to constant velocity, $x_P = v_P t$. Hence, disturbing function F_i becomes time dependent. The same expression (57) is obtained in [18] by employing the Dirac δ function for transformation of distributed load, q, to concentrated one, P.

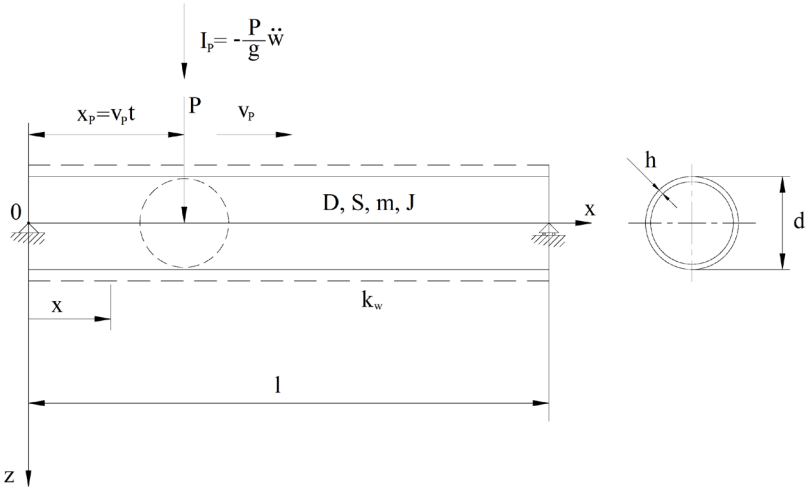

Fig. 4. Carbon nanotube embedded in elastic medium exposed to gravity and inertia force of moving nanoparticle

Sl. 4. Ugljična nanocijev uronjena u elastičnom mediju i izvrgnuta djelovanju gravitacijske i inercijske sile gibajuće nanočestice

Diagonal terms in (55) are dominant due to almost orthogonal modal functions as well as their derivatives in integrals (54). As a result, coupling of equations (55) is weak, and therefore an iteration procedure can be used for their solution. A typical

equation can be written in the form

$$N_{ii}\left(\dddot{T}_i\right)^{(k+1)} + M_{ii}\left(\ddot{T}_i\right)^{(k+1)} + K_{ii}T_i^{(k+1)} = F_i - \sum_{j=1}^{\infty}\left(1-\delta_{ij}\right)\left(N_{ij}\left(\dddot{T}_j\right)^k + M_{ij}\left(\ddot{T}_j\right)^k + K_{ij}T_j^k\right), \tag{58}$$

where δ_{ij} is the Kronecker delta and k is iteration step.

The above formulation is general for a beam with arbitrary boundary conditions, where mode function W_{bi} is expressed in terms of trigonometric and hyperbolic functions. A simply supported beam is a special case since natural modes are single trigonometric functions, i.e. $W_{bi} = \sin\dfrac{i\pi x}{l}$, and moreover they are orthogonal as well as any combination of their even derivatives. As a result, all integrals (54) are zero for $j \neq i$, and for $j = i$ they take the following values

$$I_{ii}^{(0)} = \frac{l}{2},\ I_{ii}^{(2)} = -\left(\frac{i\pi}{l}\right)^2\frac{l}{2},\ I_{ii}^{(4)} = \left(\frac{i\pi}{l}\right)^4\frac{l}{2}. \tag{59}$$

Coupling terms on the left hand side in (57) disappear and the remaining diagonal elements in (53) read

$$N_{ii} = \frac{l}{2}a_i,\ M_{ii} = \frac{l}{2}b_i,\ K_{ii} = \frac{l}{2}c_i, \tag{60}$$

where coefficients a_i, b_i and c_i are identical to $\tilde{a}$, $\tilde{b}$ and $\tilde{c}$ determined within natural vibration analysis, Eqs. (49), respectively. In this case, modal differential equation (58) takes the following form

$$N_{ii}\dddot{T}_i + M_{ii}\ddot{T}_i + K_{ii}T_i = F_i^0 \sin\Omega_i t, \tag{61}$$

where

$$F_i^0 = \frac{P}{D}\left[1+\mu\left(\frac{i\pi}{l}\right)^2\right],\ \Omega_i = \frac{i\pi v_P}{l}, \tag{62}$$

is modal excitation amplitude and forcing frequency, respectively. Assuming homogenous solution of Eq. (61) in harmonic form, $T_i^h = \sin\omega_i t$, frequency equation (48) is obtained as in the case of differential equation of motion (41). Particular integral of (61) is assumed in the same form as disturbing function

$$T_i = C_i \sin\Omega_i t, \tag{63}$$

and substituting it into (61) yields

$$C_i = \frac{F_i^0}{\Omega_i^4 N_{ii} - \Omega_i^2 M_{ii} + K_{ii}}. \tag{64}$$

Denominator in (64), according to (48), is identical to the modal frequency equation if ω_i is written instead of Ω_i. Hence, one can write

$$K_{ii} = -\omega_i^4 N_{ii} + \omega_i^2 M_{ii}, \tag{65}$$

and substituting (65) into (64) yields

$$C_i = \frac{F_i^0}{\left(\Omega_i^2 - \omega_i^2\right)\left[\left(\Omega_i^2 + \omega_i^2\right) N_{ii} - M_{ii}\right]}. \tag{66}$$

Two singular values of excitation frequency are possible, i.e. $\Omega_i = \omega_i$ and $\Omega_i = \sqrt{M_{ii}/N_{ii} - \omega_i^2}$. The former is due to translatory and the latter due to rotary inertia. Since the natural frequency spectra, Eq. (50), are quite dense, it is obvious that a particular mode can easily fall into resonance, depending on nanoparticle velocity, v_p .

In order to reduce infinite resonant response to a finite value it is necessary to include damping into differential equation of vibrations. Nanotube is supported by elastic medium and can slide along it if axial force overcomes friction force, which is equal to the product of normal force and friction coefficient. Friction force is independent on the velocity, but causes reduction of vibration amplitude due to dissipation of the kinetic energy, [34]. Therefore, damping can be modeled as a viscous one, with intensity based on equivalence of dissipated energy of friction force and the assumed viscous force, [35].

Prescribing linear viscous damping force Eq. (61) reads

$$N_{ii}\dddot{T}_i + M_{ii}\ddot{T}_i + V_{ii}\dot{T}_i + K_{ii}T_i = F_i^0 \sin\Omega_i t, \tag{67}$$

where V_{ii} is damping coefficient. Solution of (67) is assumed in the form

$$T_i = A_i \cos\Omega_i t + B_i \sin\Omega_i t. \tag{68}$$

Substituting (68) into (67) and equalizing coefficients of sine and cosine functions, system of two algebraic equations is obtained,

$$\begin{bmatrix} N_{ii}\Omega_i^4 - M_{ii}\Omega_i^2 + K_{ii} & V_{ii}\Omega_i \\ -V_{ii}\Omega_i & N_{ii}\Omega_i^4 - M_{ii}\Omega_i^2 + K_{ii} \end{bmatrix} \begin{Bmatrix} A_i \\ B_i \end{Bmatrix} = \begin{Bmatrix} 0 \\ F_i^0 \end{Bmatrix}. \tag{69}$$

Its solution, determined by the Cramer rule, reads

$$A_i = \frac{D_A^i}{D_0^i},\ B_i = \frac{D_B^i}{D_0^i}, \tag{70}$$

where

$$\begin{aligned} D_A^i &= -V_{ii}\Omega_i F_i^0, \\ D_B^i &= \left(N_{ii}\Omega_i^4 - M_{ii}\Omega_i^2 + K_{ii}\right) F_i^0, \\ D_0^i &= \left(N_{ii}\Omega_i^4 - M_{ii}\Omega_i^2 + K_{ii}\right)^2 + V_{ii}^2\Omega_i^2, \end{aligned} \tag{71}$$

are determinants of the system. Taking $C_i = \sqrt{A_i^2 + B_i^2}$, $A_i = C_i \sin\varepsilon_i$ and $B_i = C_i \cos\varepsilon_i$, Eq. (68) is transformed into the form

$$T_i = C_i \sin\left(\Omega_i t + \varepsilon_i\right), \tag{72}$$

where

$$C_i = \frac{F_i^0}{\sqrt{D_0^i}},\ \varepsilon_i = \arctan\frac{D_B^i}{D_A^i}, \tag{73}$$

is mode amplitude and phase angle, respectively. The first quantity can be presented in the well-known form for a single degree of freedom system

$$\begin{aligned} C_i &= C_{st}^i \mu_F^i,\ C_{st}^i = \frac{F_i^0}{K_{ii}}, \\ \mu_F^i &= \frac{1}{\sqrt{\left(1 - \frac{M_{ii}}{K_{ii}}\Omega_i^2 + \frac{N_{ii}}{K_{ii}}\Omega_i^4\right)^2 + \left(\frac{V_{ii}}{K_{ii}}\right)^2 \Omega_i^2}}, \end{aligned} \tag{74}$$

where C_{st}^i is modal static coefficient and μ_F^i is dynamic amplification factor. In resonances $C_i = F_i^0 / \omega_i V_{ii}$ and $\varepsilon_i = \pi/2$.

The above particular solution of Eq. (67) is steady state response and does not satisfy initial condition $T_i(0) = 0$ and $\dot{T}_i(0) = 0$. That causes transient free vibra-

tions, which are represented with homogenous solution of (67). That solution can not be obtained analytically in closed form and therefore an approximate solution is used

$$T_i^h = A_i^h \, \mathrm{e}^{-\gamma_i \omega_i t} \cos \omega_i t + B_i^h \, \mathrm{e}^{-\gamma_i \omega_i t} \sin \omega_i t, \tag{75}$$

where ω_i is natural frequency of undamped dynamic system derived in Section 4.3, and $\gamma_i = V_{ii} \big/ \left(2 \omega_i M_{ii} \right)$ is nondimensional damping coefficient.

Particular solution of (67) is presented with (68), and total time function is $T_i^* = T_i^h + T_i$. Constants A_i^h and B_i^h are determined by satisfying initial conditions $T_i^* \left(0 \right) = 0$ and $\dot{T}_i^* \left(0 \right) = 0$,

$$A_i^h = -A_i, \; B_i^h = -\frac{\Omega_i}{\omega_i} B_i - \gamma_i A_i. \tag{76}$$

Hence, the complete time function yields

$$\begin{aligned} T_i^* = {} & A_i \left[\cos \Omega_i t - e^{-\gamma_i \omega_i t} \left(\cos \omega_i t + \gamma_i \sin \omega_i t \right) \right] \\ & + B_i \left(\sin \Omega_i t - \frac{\Omega_i}{\omega_i} e^{-\gamma_i \omega_i t} \sin \omega_i t \right). \end{aligned} \tag{77}$$

In resonance $\Omega_i = \omega_i$ and according to Eqs. (70) and (71) $A_i = -F_i^0 \big/ \left(2 \gamma_i \omega_i^2 \right)$ and $B_i = 0$, and Eq. (77) is reduced to

$$T_{i\mathrm{res}}^* = \frac{F_i^0}{2 \omega_i^2 M_{ii}} \left[\frac{1}{\gamma_i} \left(e^{-\gamma_i \omega_i t} - 1 \right) \cos \omega_i t + e^{-\gamma_i \omega_i t} \sin \omega_i t \right]. \tag{78}$$

In case of conservative dynamic system, $\gamma_i = 0$, the second term in (78) is determined, while the first one takes undetermined form, i.e. $T_{i\mathrm{res}}^{*(1)} = \mathrm{Nom} / \mathrm{Denom} = 0/0$. That is only apparently, and the problem can be overcome if the exponential function is expanded into the power series $e^{-\gamma_i \omega_i t} = 1 - \gamma_i \omega_i t + \frac{1}{2} \left(\gamma_i \omega_i t \right)^2 \mp \ldots$. Hence, one finds

$$T_{i\mathrm{res}}^* = \frac{F_i^0}{2 \omega_i^2 M_{ii}} \left[e^{-\gamma_i \omega_i t} \sin \omega_i t - \omega_i t \left(1 - \frac{1}{2} \gamma_i \omega_i t \right) \cos \omega_i t \right]. \tag{79}$$

If $\gamma_i = 0$, Eq. (79) takes a simpler form

$$T_{i\mathrm{res}}^* = \frac{F_i^0}{2 \omega_i^2 M_{ii}} \left(\sin \omega_i t - \omega_i t \cos \omega_i t \right). \tag{80}$$

While damping plays decisive role in resonant steady state response, which attains infinite value if damping is not present, Eq. (74), the resonant response starting from the rest is a smooth function. That is a reason why numerical time integration of differential equation of motion without damping force can be performed in resonance without difficulties.

It is obvious from (80) that envelope of amplitude is increased linearly by time to infinity. Since passing time of nanoparticle through nanotube is known, $t_P = l/v_P$, and $\Omega_i = i\pi v_P/l = \omega_i$, yields $\omega_i t_P = i\pi$. It means that number of time function half waves is equal to the mode number i. The time function achieves its maximum value at t_P, i.e. $T_{i\mathrm{res}}^{*(\max)} = i\pi F_i^0 \left/ \left(2\omega_i^2 M_{ii}\right)\right.$.

4.4 Numerical example

4.4.1 Basic data

Application of the presented theory is illustrated in the case of simply supported embedded SWCNT exposed to the influence of moving nanoparticle gravity load. Values of the basic parameters are chosen the same as in [18] in order to enable comparison of some results: Young's modulus $E = 1\ \mathrm{TPa}\ = 10^3\ \mathrm{nN/(nm)}^2$, mass density $\rho = 2300\ \mathrm{kg/m}^3 = 2.3\cdot 10^{-15}\ \mathrm{nkg/(nm)}^3$, outer diameter $d = 1\ \mathrm{nm}$, wall thickness $h = 0.34\ \mathrm{nm}$ and Poisson's ratio $\nu = 0.2$. The derived data are the following: cross-section area $A = d^2\pi/4 = 0.70497\ \ (\mathrm{nm})^2$, moment of inertia of cross-section $I = \left[d^4 - (d-2h)^4\right]\pi \left/ 64 = 0.048573\ \ (\mathrm{nm})^4\right.$. The shear correction factor for hollow circle is determined according to [31], $k_s = 0.71376$. Values of nanotube length, l, stiffness of elastic medium, k_w, and nonlocal parameter, μ, are varied.

4.4.2 Natural vibrations

Natural frequencies for simply supported SWCNT are calculated according to Eq. (50), for different values of slenderness ratio l/d and nonlocal parameter μ. They are normalized by the first natural frequency of the simply supported Euler-Bernoulli beam, $\omega_{EB}^1 = (\pi/l)^2\sqrt{EI/\rho A}$, so that frequency parameter reads $\lambda_i = \pi^2\omega_i/\omega_{EB}^1 = \omega_i l^2\sqrt{\rho A/EI}$. The obtained results for the first natural mode are listed in Table 1, [18] and compared with those from Refs. [18] and [21]. Values from Ref. [21] agree excellently with analytical ones, while those from Ref. [18] are slightly different.

Influence of elastic medium stiffness , k_w, on nanotube natural frequencies can be seen in Table 2. Values of frequency parameters are somewhat increased for higher stiffness as expected.

Table 1 - The first frequency parameter $\lambda_1 = \omega_1 l^2 \sqrt{\rho A/EI}$ for simply supported nanotube, $k_w = 0$, $k_s = 5/6$

l/d	μ (nm)	PS	Ref. [21]	Ref. [18]
10	0	9.7425	9.7443	9.7074
	1	9.2974	9.2931	9.2612
	2	8.9081	8.8994	8.8713
	3	8.5640	8.5517	8.5268
	4	8.2569	8.2419	8.2196
20	0	9.8373	9.8381	9.8281
	1	9.7183	9.7187	9.7090
	2	9.6035	9.6036	9.5942
	3	9.4928	9.4924	9.4834
	4	9.3857	9.3850	9.3763
50	0	9.8644	9.8645	9.8629
	1	9.8450	9.8451	9.8435
	2	9.8257	9.8258	9.8242
	3	9.8065	9.8066	9.8050
	4	9.7875	9.7875	9.7859

Table 2 - Frequency parameter $\lambda_i = \omega_i l^2 \sqrt{\rho A/EI}$ for simply supported nanotube, $l/d = 10$, $k_s = 0.71376$, $\mu = 0$

Mode no.	$k_w = 0$	$k_w = 10^{-5}\ E$	$k_w = 10^{-4}\ E$
1	9.7271	9.8317	10.7271
2	37.3631	37.3900	37.6315
3	79.2282	79.2406	79.3527
4	131.2700	131.2770	131.3430
5	190.1420	190.1470	190.1920
6	253.4390	253.4430	253.4760
7	319.5350	319.5380	319.5640
8	387.3590	387.3610	387.3830
9	456.2120	456.2140	456.2330
10	525.6390	525.6410	525.6580

4.4.3 Forced vibrations

Forced vibrations of SWCNT are performed by employing procedure presented in Section 4.3. Some vibration parameters are normalized. Modal damping coefficient is specified as $V_{ii} = 2\gamma_i \omega_i M_{ii}$, where γ_i is nondimensional parameter. Velocity pa-

rameter is defined as ratio of nanoparticle velocity and velocity which corresponds to the first natural mode of nanotube, i.e. $\alpha = v_P / v_1 = \Omega_1 / \omega_1 = \pi v_P / (\omega_1 l)$. Nondimensional time is $\tau = x_P / l = v_P t / l$. Vibration deflection is normalized by the static value due to lumped force P acting at the midsection, i.e. $\delta(x,t) = w(x,t) / w_P$, where $w_P = Pl^3 / 48EI$.

All numerical calculations for forced vibrations are performed by employing 30 natural modes, that was necessary to stabilize the first 6 digits of response. Fig. 5 shows time history of maximum relative deflection of nanotube during nanoparticle motion from the rest, $t = 0$, up to passing time, t_P. Relief presentation points out moving of maximum deflection simultaneously with nanoparticle. Maximum relative deflection as function of velocity parameter, determined by step $\Delta\alpha = 0.01$, is shown in Fig. 6. Response is rapidly increased for higher values of $\sqrt{\mu}$.

Influence of damping response is analyzed in case of resonance, $\alpha = 1$. Time history of relative midsection deflection within time period of double value of passing time of nanoparticle is shown in Fig. 7. Response is dominated by the first natural mode, especially for higher damping value. Reason is that damping force is proportional to natural frequency, $V_{ii} = 2\gamma_i \omega_i$. Contribution of the other natural modes is more pronounced when there is no damping.

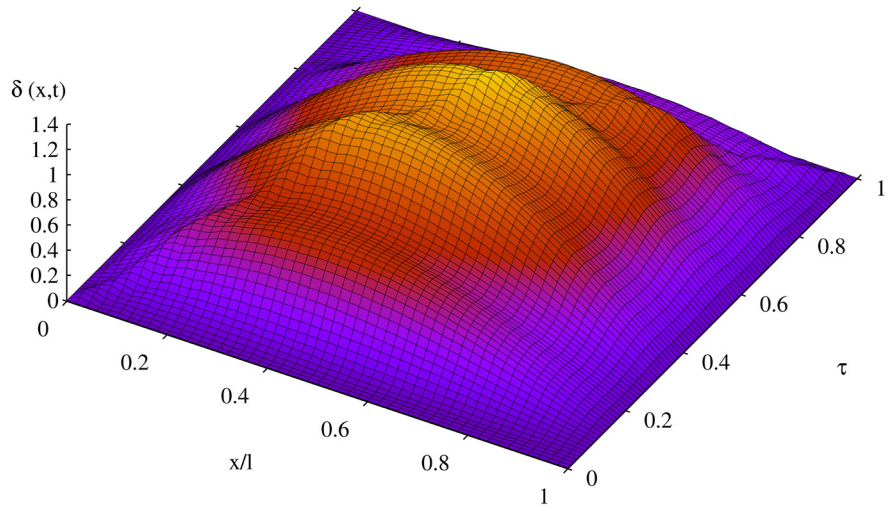

Fig. 5. Time history of relative deflection of nanotube, $l/d = 10$, $k_w = 0$, $P/g = 0$, $\sqrt{\mu}$ = 1 nm, $\alpha = 0.1$, $\gamma_i = 0.0$

Sl. 5. Vremenska promjena relativnog gibanja nanocijevi, $l/d = 10$, $k_w = 0$, $P/g = 0$, $\sqrt{\mu}$ = 1 nm, $\alpha = 0.1$, $\gamma_i = 0.0$

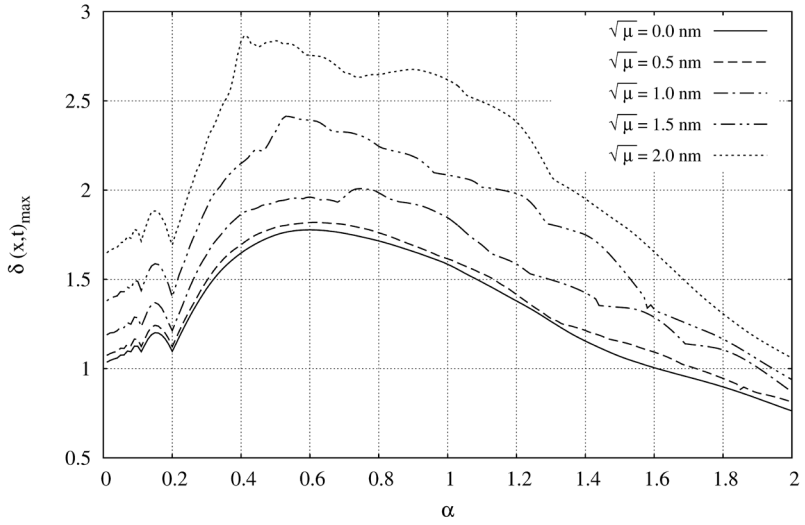

Fig. 6. Maximum relative deflection versus velocity parameter, $l/d=10,\ k_w=0,\ P/g=0,\ \gamma_i=0.0$

Sl. 6. Maksimalni relativni progib u ovisnosti o parametru brzine, $l/d=10,\ k_w=0,\ P/g=0,\ \gamma_i=0.0$

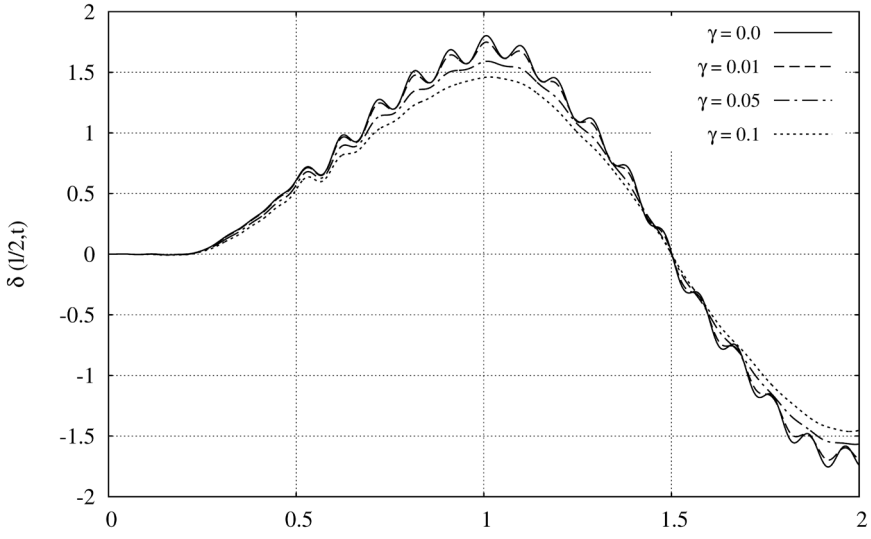

Fig. 7. Time history of relative midsection deflection in resonance,
$l/d=10,\ \alpha=1,\ k_w=10^{-5}E\ ,\sqrt{\mu}\ =1\ \text{nm},\ P/g=0$

Sl. 7. Vremenska promjena relativnog gibanja po sredini nanocijevi u rezonanciji

5. COUPLED HORIZONTAL AND TORSIONAL VIBRATIONS OF ULTRA LARGE SHIPS

5.1 General

Increased sea transport requires building of ultra large container ships which are quite flexible. Therefore, their strength has to be checked by hydroelastic analysis [36]. The methodology of hydroelastic analysis is described in [37]. It includes the definition of the structural model, ship and cargo mass distributions, and geometrical model of ship wetted surface. Hydroelastic analysis is based on the modal superposition method. First, dry natural vibrations of ship hull are calculated. Then, modal hydrostatic stiffness, modal added mass, modal damping and modal wave load are determined. Finally, the calculation of wet natural vibrations is performed and transfer functions for determining ship structural response to wave excitation are obtained [38].

The intention of this Section is to present an advanced numerical procedure based on the beam and thin-walled girder theories for reliable calculation of dry natural vibrations of container ships, as an important step in their hydroelastic analysis. A ship hull, as an elastic nonprismatic thin-walled girder, performs longitudinal, vertical, horizontal and torsional vibrations. Since the cross-sectional centre of gravity and centroid, as well as the shear centre positions are not identical, coupled longitudinal and vertical, and horizontal and torsional vibrations occur, respectively.

The distance between the centre of gravity and centroid for longitudinal and vertical vibrations, as well as distance between the former and shear centre for horizontal and torsional vibrations are negligible for conventional ships. Therefore, in the above cases ship hull vibrations are usually analysed separately. However, the shear centre in ships with large hatch openings is located outside the cross-section, i.e. below the keel, and therefore the coupling of horizontal and torsional vibrations is extremely high.

The above problem is rather complicated due to geometrical discontinuity of the hull cross-section. The accuracy of the solution depends on the reliability of stiffness parameters determination, i.e. of bending, shear, torsional and warping moduli. The finite element method is a powerful tool to solve the above problem in a successful way. One of the first solutions for coupled horizontal and torsional hull vibrations, dealing with the finite element technique, is given in [39,40]. Generalised and improved solutions are presented in [41,42]. An advanced theory of thin-walled girder with application to ship vibrations is worked out in [30].

5.2 Differential equations of beam vibrations

Referring to the flexural beam theory [31], the total beam deflection, w, consists of the bending deflection, w_b, and the shear deflection, w_s, while the angle of cross-section rotation depends only on the former, Fig. 8

$$w = w_b + w_s, \quad \varphi = \frac{\partial w_b}{\partial x}. \tag{81}$$

The cross-sectional forces are the bending moment and the shear force

$$M = -EI_b \frac{\partial \varphi}{\partial x}, \; Q = GA_s \frac{\partial w_s}{\partial x}, \tag{82}$$

where E and G are the Young's and shear modulus, respectively, while I_b and A_s are the moment of inertia of cross-section and shear area, respectively.

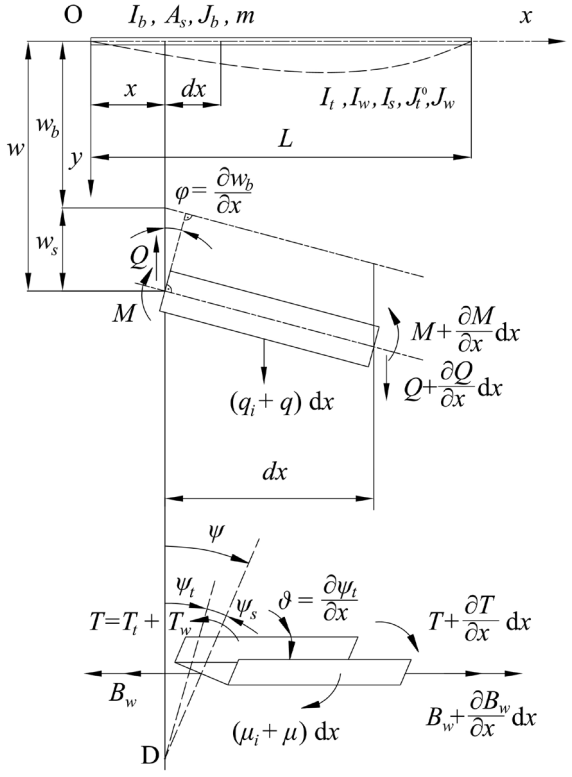

Fig. 8. Beam bending and torsion

Sl. 8. Savijanje i uvijanje grede

The inertia load consists of the distributed transverse load, q_i, and the bending moment, μ_i, and in the case of coupled horizontal and torsional vibration is specified as

$$q_i = -m\left(\frac{\partial^2 w}{\partial t^2} + c\frac{\partial^2 \psi}{\partial t^2}\right),\ \mu_i = -J_b\frac{\partial^2 \varphi}{\partial t^2}, \tag{83}$$

where m is the distributed ship and added mass, J_b is the moment of inertia of ship mass about z-axis, and c is the distance between the centre of gravity and the shear centre, $c = z_G - z_S$, Fig 9.

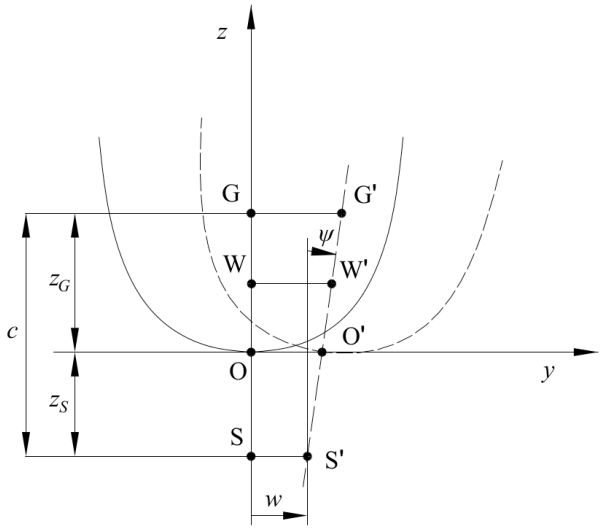

Fig. 9. Cross-section of a thin-walled girder

Sl. 9. Poprečni presjek tankostijenog nosača

Concerning torsion, the total twist angle, ψ (which should be distinguished from the cross-section rotation, ψ, within the Timoshenko beam theory, Sections 2 and 3), consists of the pure twist angle, ψ_t, and the shear contribution, ψ_s, while the second beam displacement, which causes warping (deplanation) of cross-section, is variation of the pure twist angle, i.e. Fig. 8 [30]

$$\psi = \psi_t + \psi_s,\ \vartheta = \frac{\partial \psi_t}{\partial x}. \tag{84}$$

The cross-sectional forces include the pure torsional torque, T_t, warping bimoment, B_w, and additional torque due to restrained warping, T_w, i.e.

$$T_t = GI_t\vartheta,\ B_w = -EI_w\frac{\partial\vartheta}{\partial x},\ T_w = GI_s\frac{\partial\psi_s}{\partial x},, \tag{85}$$

where I_t, I_w and I_s are the torsional modulus, warping modulus and shear inertia modulus, respectively.

The inertia load consists of the distributed torque, μ_{ti}, and the bimoment, b_i, presented in the following form:

$$\mu_{ti} = -J_t\frac{\partial^2\psi}{\partial t^2} - mc\frac{\partial^2 w}{\partial t^2},\ b_i = -J_w\frac{\partial^2\vartheta}{\partial t^2}, \tag{86}$$

where J_t is the polar moment of inertia of ship and added mass about the shear centre, and J_w is the bimoment of inertia of ship mass about the warping centre, Fig. 9.

Considering the equilibrium of a differential element, one can write for flexural vibrations

$$\frac{\partial M}{\partial x} = Q + \mu_i,\ \frac{\partial Q}{\partial x} = -q_i - q, \tag{87}$$

and for torsional vibrations [29]

$$\frac{\partial B_w}{\partial x} = T_w + b_i,\ \frac{\partial T_t}{\partial x} + \frac{\partial T_w}{\partial x} = -\mu_{ti} - \mu. \tag{88}$$

The above equations can be reduced to two coupled partial differential equations as follows. Substituting Eqs. (82) into the first of Eqs. (87) yields

$$\frac{\partial w_s}{\partial x} = -\frac{EI_b}{GA_s}\frac{\partial^2\varphi}{\partial x^2} + \frac{J_b}{GA_s}\frac{\partial^2\varphi}{\partial t^2}. \tag{89}$$

By inserting the second of Eqs. (82) and the first of (83) into the second of (87) leads

$$EI_b\frac{\partial^4\varphi}{\partial x^4} + m\frac{\partial^2\varphi}{\partial t^2} - \left(J_b + m\frac{EI_b}{GA_s}\right)\frac{\partial^4\varphi}{\partial x^2\partial t^2} + \frac{mJ_b}{GA_s}\frac{\partial^4\varphi}{\partial t^4} + mc\frac{\partial^3\psi}{\partial x\partial t^2} = \frac{\partial q}{\partial x}. \tag{90}$$

In similar way, substituting the second and third of Eqs. (85) into the first of Eqs. (88) yields

$$\frac{\partial\psi_s}{\partial x} = -\frac{EI_w}{GI_s}\frac{\partial^2\vartheta}{\partial x^2} + \frac{J_w}{GI_s}\frac{\partial^2\vartheta}{\partial t^2}. \tag{91}$$

By inserting Eqs. (85) into the second of Eqs. (88) one finds

$$EI_w \frac{\partial^4 \vartheta}{\partial x^4} - GI_t \frac{\partial^2 \vartheta}{\partial x^2} + J_t \frac{\partial^2 \vartheta}{\partial t^2} - \left(J_w + J_t \frac{EI_w}{GI_s} \right) \frac{\partial^4 \vartheta}{\partial x^2 \partial t^2} + \frac{J_w}{GI_s} \frac{\partial^4 \vartheta}{\partial t^4} + mc \frac{\partial^3 w}{\partial x \partial t^2} = \frac{\partial \mu}{\partial x} \tag{92}$$

Furthermore, ψ in (90) can be split into $\psi_t + \psi_s$ and the later term can be expressed with (91). Similar substitution can be done for $w = w_b + w_s$ in (92), where w_s is given with (89). Thus, taking into account that $\varphi = \partial w_b / \partial x$ and $\vartheta = \partial \psi_t / \partial x$, Eqs (90) and (92) after integration per x read

$$EI_b \frac{\partial^4 w_b}{\partial x^4} + m \frac{\partial^2 w_b}{\partial t^2} - \left(J_b + m \frac{EI_b}{GA_s} \right) \frac{\partial^4 w_b}{\partial x^2 \partial t^2} + \frac{mJ_b}{GA_s} \frac{\partial^4 w_b}{\partial t^4} + mc \left(\frac{\partial^2 \psi_t}{\partial t^2} - \frac{EI_w}{GI_s} \frac{\partial^4 \psi_t}{\partial x^2 \partial t^2} + \frac{J_w}{GI_s} \frac{\partial^4 \psi_t}{\partial t^4} \right) = q \tag{93}$$

$$EI_w \frac{\partial^4 \psi_t}{\partial x^4} - GI_t \frac{\partial^2 \psi_t}{\partial x^2} + J_t \frac{\partial^2 \psi_t}{\partial t^2} - \left(J_w + J_t \frac{EI_w}{GI_s} \right) \frac{\partial^4 \psi_t}{\partial x^2 \partial t^2} + \frac{J_w}{GI_s} \frac{\partial^4 \psi_t}{\partial t^4} + mc \left(\frac{\partial^2 w_b}{\partial t^2} - \frac{EI_b}{GA_s} \frac{\partial^4 w_b}{\partial x^2 \partial t^2} + \frac{J_b}{GA_s} \frac{\partial^4 w_b}{\partial t^4} \right) = \mu. \tag{94}$$

After solving Eqs. (93) and (94) the total deflection and twist angle are obtained by employing (89) and (91)

$$w = w_b + w_s = w_b - \frac{EI_b}{GA_s} \frac{\partial^2 w_b}{\partial x^2} + \frac{J_b}{GA_s} \frac{\partial^2 w_b}{\partial t^2} + f(t) \tag{95}$$

$$\psi = \psi_t + \psi_s = \psi_t - \frac{EI_w}{GI_s} \frac{\partial^2 \psi_t}{\partial x^2} + \frac{J_w}{GI_s} \frac{\partial^2 \psi_t}{\partial t^2} + g(t), \tag{96}$$

where f(t) and g(t) are integration functions, which depend on initial conditions.

The main purpose of developing differential equations of vibrations (93) and (94) is to get insight into their constitution, position and role of the stiffness and mass parameters, and coupling, which is realized through the inertia terms. If the pure torque T_t is excluded from the above theoretical consideration, it is obvious that the complete analogy between bending and torsion exists, [43].

Application of Eqs. (93) and (94) is limited to prismatic girders. For more complex problems, like ship hull, the finite element method, as a powerful tool, is on disposal.

The shape functions of beam finite element for vibration analysis have to satisfy the following consistency relations for harmonic vibrations obtained from Eqs. (95) and (96), [44]

$$w = w_b + w_s = \left(1 - \omega^2 \frac{J_b}{GA_s}\right) w_b - \frac{EI_b}{GA_s} \frac{\mathrm{d}^2 w_b}{\mathrm{d}x^2} \tag{97}$$

$$\psi = \psi_t + \psi_s = \left(1 - \omega^2 \frac{J_w}{GI_s}\right) \psi_t - \frac{EI_w}{GI_s} \frac{\mathrm{d}^2 \psi_t}{\mathrm{d}x^2}. \tag{98}$$

5.3 Beam finite element

The properties of a finite element for the coupled flexural horizontal and torsional vibration analysis can be derived from the total element energy. The total energy consists of the strain energy, the kinetic energy, the work of the external lateral load, q, and the torque, μ, and the work of the boundary forces. Thus, according to [40, 44],

$$\begin{aligned} E_{tot} = {} & \frac{1}{2}\int_0^l \left[EI_b \left(\frac{\partial^2 w_b}{\partial x^2}\right)^2 + GA_s \left(\frac{\partial w_s}{\partial x}\right)^2 + EI_w \left(\frac{\partial^2 \psi_t}{\partial x^2}\right)^2 + GI_s \left(\frac{\partial \psi_s}{\partial x}\right)^2 + GI_t \left(\frac{\partial \psi_t}{\partial x}\right)^2 \right] \mathrm{d}x \\ & + \frac{1}{2}\int_0^l \left[m \left(\frac{\partial w}{\partial t}\right)^2 + J_b \left(\frac{\partial^2 w_b}{\partial x \partial t}\right)^2 + 2mc \frac{\partial w}{\partial t}\frac{\partial \psi}{\partial t} + J_w \left(\frac{\partial^2 \psi_t}{\partial x \partial t}\right)^2 + J_t \left(\frac{\partial \psi}{\partial t}\right)^2 \right] \mathrm{d}x \\ & - \int_0^l (qw + \mu\psi)\mathrm{d}x + (Qw - M\varphi + T\psi + B_w \vartheta)_0^l, \end{aligned} \tag{99}$$

where l is the element length.

Since the beam has four displacements, $w, \varphi, \psi, \vartheta$, a two-node finite element has eight degrees of freedom, i.e. four nodal shear-bending and torsion-warping displacements respectively, Fig. 10,

$$\{U\} = \begin{Bmatrix} w(0) \\ \varphi(0) \\ w(l) \\ \varphi(l) \end{Bmatrix}, \quad \{V\} = \begin{Bmatrix} \psi(0) \\ \vartheta(0) \\ \psi(l) \\ \vartheta(l) \end{Bmatrix}. \tag{100}$$

Therefore, the basic beam displacements, w_b and ψ_t, can be presented as the third-order polynomials

$$\begin{aligned} & w_b = \langle a_k \rangle \{\xi^k\}, \ \psi_t = \langle d_k \rangle \{\xi^k\}, \ k = 0,1,2,3, \\ & \xi = \frac{x}{l}, \ \langle \dots \rangle = \{\dots\}^T. \end{aligned} \tag{101}$$

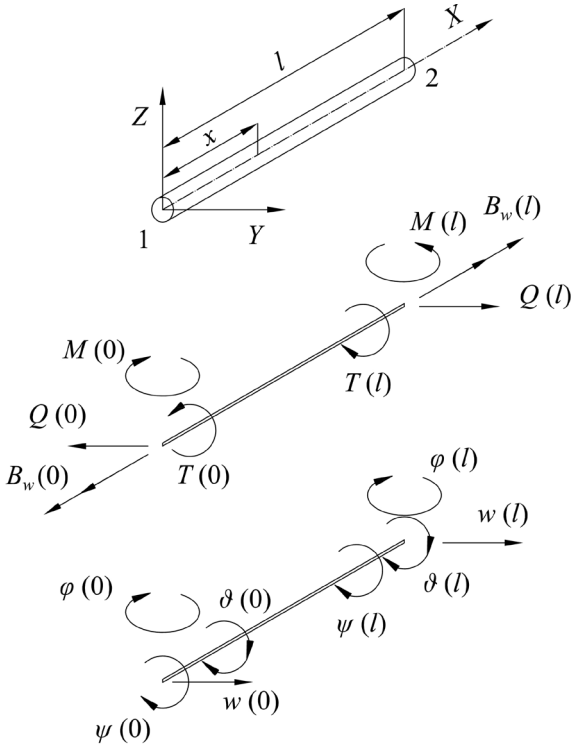

Fig. 10. Beam finite element

Sl. 10. Gredni konačni element

Furthermore, satisfying alternately the unit value for one of the nodal displacement $\{U\}$ and zero values for the remaining displacements, and doing the same for $\{V\}$, it follows that:

$$\begin{aligned} &w_b = \langle w_{bi} \rangle \{U\},\ w_s = \langle w_{si} \rangle \{U\},\ w = \langle w_i \rangle \{U\}, \\ &\psi_t = \langle \psi_{ti} \rangle \{V\},\ \psi_s = \langle \psi_{si} \rangle \{V\},\ \psi = \langle \psi_i \rangle \{V\},\ i = 1,2,3,4, \end{aligned} \tag{102}$$

where w_{bi}, w_{si}, w_i and ψ_{ti}, ψ_{si}, ψ_i are the shape functions specified below by employing relations (97) and (98)

$$\begin{aligned} &w_{bi} = \langle a_{ik} \rangle \{\xi^k\},\ w_{si} = \langle b_{ik} \rangle \{\xi^k\},\ w_i = \langle c_{ik} \rangle \{\xi^k\} \\ &\psi_{ti} = \langle d_{ik} \rangle \{\xi^k\},\ \psi_{si} = \langle e_{ik} \rangle \{\xi^k\},\ \psi_i = \langle f_{ik} \rangle \{\xi^k\} \end{aligned} \tag{103}$$

$$[a_{ik}]=\frac{1}{\alpha(\alpha+12\beta)}\begin{bmatrix}\alpha+6\beta & 0 & -3\alpha & 2\alpha\\ -4\beta(\alpha+3\beta)l & \alpha(\alpha+12\beta)l & -2\alpha(\alpha+3\beta)l & \alpha^2 l\\ 6\beta & 0 & 3\alpha & -2\alpha\\ -2\beta(\alpha-6\beta)l & 0 & -\alpha(\alpha-6\beta)l & \alpha^2 l\end{bmatrix} \tag{104}$$

$$\begin{aligned} b_{i0}&=-(1-\alpha)a_{i0}-2\beta a_{i2}\\ b_{i1}&=-(1-\alpha)a_{i1}-6\beta a_{i3}\\ b_{i2}&=-(1-\alpha)a_{i2}\\ b_{i3}&=-(1-\alpha)a_{i3}, \end{aligned} \tag{105}$$

$$[c_{ik}]=[a_{ik}]+[b_{ik}],\quad i=1,2,3,4,\quad k=0,1,2,3 \tag{106}$$

$$\alpha=1-\omega^2\frac{J_b}{GA_s},\ \beta=\frac{EI_b}{GA_s l^2} \tag{107}$$

Constitution of torsional matrices $[d_{ik}]$, $[e_{ik}]$ and $[f_{ik}]$ is the same as $[a_{ik}]$, $[b_{ik}]$ and $[c_{ik}]$, but parameters α and β have to be exchanged with

$$\eta=1-\omega^2\frac{J_w}{GI_s},\ \gamma=\frac{EI_w}{GI_s l^2} \tag{108}$$

according to (98).

By substituting Eqs. (102) into (99) one obtains

$$E_{tot}=\frac{1}{2}\begin{Bmatrix}U\\V\end{Bmatrix}^T\begin{bmatrix}k_{bs} & 0\\ 0 & k_{ws}+k_t\end{bmatrix}\begin{Bmatrix}U\\V\end{Bmatrix}+\frac{1}{2}\begin{Bmatrix}\dot U\\ \dot V\end{Bmatrix}^T\begin{bmatrix}m_{sb} & m_{st}\\ m_{ts} & m_{tw}\end{bmatrix}\begin{Bmatrix}\dot U\\ \dot V\end{Bmatrix}-\begin{Bmatrix}q\\ \mu\end{Bmatrix}^T\begin{Bmatrix}U\\V\end{Bmatrix}-\begin{Bmatrix}P\\R\end{Bmatrix}^T\begin{Bmatrix}U\\V\end{Bmatrix}, \tag{109}$$

where, assuming constant values of the element properties,

$$[k]_{bs}=\left[EI_b\int_0^l\frac{\mathrm{d}^2w_{bi}}{\mathrm{d}x^2}\frac{\mathrm{d}^2w_{bj}}{\mathrm{d}x^2}\mathrm{d}x+GA_s\int_0^l\frac{\mathrm{d}w_{si}}{\mathrm{d}x}\frac{\mathrm{d}w_{sj}}{\mathrm{d}x}\mathrm{d}x\right]$$ – bending-shear stiffness matrix,

$$[k]_{ws}=\left[EI_w\int_0^l\frac{\mathrm{d}^2\psi_{ti}}{\mathrm{d}x^2}\frac{\mathrm{d}^2\psi_{tj}}{\mathrm{d}x^2}\mathrm{d}x+GI_s\int_0^l\frac{\mathrm{d}\psi_{si}}{\mathrm{d}x}\frac{\mathrm{d}\psi_{sj}}{\mathrm{d}x}\mathrm{d}x\right]$$ – warping-shear stiffness matrix,

$$[k]_t = \left[GI_t \int_0^l \frac{\mathrm{d}\psi_{ti}}{\mathrm{d}x} \frac{\mathrm{d}\psi_{tj}}{\mathrm{d}x} \mathrm{d}x \right] - \text{torsion stiffness matrix,}$$

$$[m]_{sb} = \left[m \int_0^l w_i w_j \mathrm{d}x + J_b \int_0^l \frac{\mathrm{d}w_{bi}}{\mathrm{d}x} \frac{\mathrm{d}w_{bj}}{\mathrm{d}x} \mathrm{d}x \right] - \text{shear-bending mass matrix,}$$

$$[m]_{tw} = \left[J_t \int_0^l \psi_i \psi_j \mathrm{d}x + J_w \int_0^l \frac{\mathrm{d}\psi_{ti}}{\mathrm{d}x} \frac{\mathrm{d}\psi_{tj}}{\mathrm{d}x} \mathrm{d}x \right] - \text{torsion-warping mass matrix,}$$

$$[m]_{st} = \left[mc \int_0^l w_i \psi_j \mathrm{d}x \right], \quad [m]_{ts} = [m]_{st}^T - \text{shear-torsion mass matrix,}$$

$$\{q\} = \left\{ \int_0^l q\, w_j \, \mathrm{d}x \right\} - \text{shear load vector,}$$

$$\{\mu\} = \left\{ \int_0^l \mu \psi_j \, \mathrm{d}x \right\} - \text{torsion load vector,} \tag{110}$$

The vectors {*P*} and {*R*} represent the shear-bending and torsion-warping nodal forces, respectively,

$$\{P\} = \begin{Bmatrix} -Q(0) \\ M(0) \\ Q(l) \\ -M(l) \end{Bmatrix}, \quad \{R\} = \begin{Bmatrix} -T(0) \\ B_w(0) \\ T(l) \\ -B_w(l) \end{Bmatrix}. \tag{111}$$

The above matrices are specified in [30], as well as the load vectors for linearly distributed loads along the element, i.e.

$$q = q_0 + q_1 \xi, \quad \mu = \mu_0 + \mu_1 \xi \,. \tag{112}$$

Shape functions of sectional forces are also given in [30].

The total element energy has to be at its minimum. Satisfying the relevant conditions

$$\frac{\partial E_{tot}}{\partial \{U\}} = \{0\}, \quad \frac{\partial E_{tot}}{\partial \{V\}} = \{0\} \tag{113}$$

and by employing the Lagrange equations of motion, the finite element equation yields

$$\{f\} = [k]\{\delta\} + [m]\{\ddot{\delta}\} - \{f\}_{q\mu}, \tag{114}$$

where

$$\{f\} = \begin{Bmatrix} P \\ R \end{Bmatrix}, \quad \{f\}_{q\mu} = \begin{Bmatrix} q \\ \mu \end{Bmatrix}, \quad \{\delta\} = \begin{Bmatrix} U \\ V \end{Bmatrix}$$
$$[k] = \begin{bmatrix} k_{bs} & 0 \\ 0 & k_{ws} + k_t \end{bmatrix}, \quad [m] = \begin{bmatrix} m_{sb} & m_{st} \\ m_{ts} & m_{tw} \end{bmatrix}. \tag{115}$$

It is obvious that coupling between the bending and torsion occurs through the mass matrix only, i.e. by the coupling matrices $[m]_{st}$ and $[m]_{ts}$.

In the finite element equation (114), first the element properties related to bending and then those related to torsion appear. To make an ordinary finite element assembling possible, it is necessary to transform Eq. (114) in such a way that first all properties related to the first node are specified and then those belonging to the second one. Thus, the rearranged nodal force and displacement vectors read

$$\{\tilde{f}\} = \begin{Bmatrix} -Q(0) \\ M(0) \\ -T(0) \\ B_w(0) \\ Q(l) \\ -M(l) \\ T(l) \\ -B_w(l) \end{Bmatrix}, \quad \{\tilde{\delta}\} = \begin{Bmatrix} w(0) \\ \varphi(0) \\ \psi(0) \\ \varphi(0) \\ w(l) \\ \varphi(l) \\ \psi(l) \\ \varphi(l) \end{Bmatrix}. \tag{116}$$

The same transformation has to be done for the load vector $\{f\}_{q\mu}$ resulting in $\{\tilde{f}\}_{q\mu}$. The above vector transformation implies also the row and column exchange in the stiffness and mass matrices.

The element deflection refers to the shear centre as the origin of a local coordinate system. Since the vertical position of the shear centre varies along the ship's hull, it is necessary to prescribe the element deflection for a common line, in order to be able to assemble the elements. Thus, choosing the x-axis (base line) of the global coordinate system as the referent line, the following relation between the former and the latter nodal deflections exists:

$$\begin{aligned} w(0) &= \overline{w}(0) + z_S\psi(0) \\ w(l) &= \overline{w}(l) + z_S\psi(l), \end{aligned} \tag{117}$$

where z_S is the coordinate of the shear centre, Fig. 9. Other displacements are the same in both coordinate systems. Twist angle ψ does not have influence on the cross-section rotation angle φ. The local displacement vector can be expressed as

$$\left\{\tilde{\delta}\right\} = \left[\tilde{T}\right]\left\{\overline{\tilde{\delta}}\right\}, \tag{118}$$

where $\left[\tilde{T}\right]$ is the transformation matrix

$$\left[\tilde{T}\right] = \begin{bmatrix} [T] & [0] \\ [0] & [T] \end{bmatrix}, \quad [T] = \begin{bmatrix} 1 & 0 & z_S & 0 \\ 0 & 1 & 0 & 0 \\ 0 & 0 & 1 & 0 \\ 0 & 0 & 0 & 1 \end{bmatrix}. \tag{119}$$

Since the total element energy is not changed by the above transformations, a new element equation can be derived taking (118) into account. Thus, one obtains in the global coordinate system

$$\left\{\overline{\tilde{f}}\right\} = \left[\overline{\tilde{k}}\right]\left\{\overline{\tilde{\delta}}\right\} + \left[\overline{\tilde{m}}\right]\left\{\ddot{\overline{\tilde{\delta}}}\right\} - \left\{\overline{\tilde{f}}\right\}_{q\mu}, \tag{120}$$

where

$$\begin{aligned} \left\{\overline{\tilde{f}}\right\} &= \left[\tilde{T}\right]^T\left\{\tilde{f}\right\} \\ \left[\overline{\tilde{k}}\right] &= \left[\tilde{T}\right]^T\left[\tilde{k}\right]\left[\tilde{T}\right] \\ \left[\overline{\tilde{m}}\right] &= \left[\tilde{T}\right]^T\left[\tilde{m}\right]\left[\tilde{T}\right] \\ \left\{\overline{\tilde{f}}\right\}_{q\mu} &= \left[\tilde{T}\right]^T\left\{\tilde{f}\right\}_{q\mu}. \end{aligned} \tag{121}$$

The first of the above expressions transforms the nodal torques into the form

$$\begin{aligned} -\overline{T}(0) &= -T(0) - z_S Q(0) \\ \overline{T}(l) &= T(l) + z_S Q(l). \end{aligned} \tag{122}$$

5.4 Numerical procedure for vibration analysis

A ship's hull is modelled by a set of beam finite elements. Their assemblage in the global coordinate system, performed in the standard way, results in the matrix equation of motion, which may be extended by the damping forces

$$[K]\{\Delta\}+[C]\{\dot{\Delta}\}+[M]\{\ddot{\Delta}\}=\{F(t)\}, \tag{123}$$

where [*K*], [*C*] and [*M*] are the stiffness, damping and mass matrices, respectively; $\{\Delta\}, \{\dot{\Delta}\}$ and $\{\ddot{\Delta}\}$ are the displacement, velocity and acceleration vectors, respectively; and {*F*(*t*)} is the load vector.

In case of natural vibration {*F*(*t*)} = {0} and the influence of damping is rather low for ship structures, so that the damping forces may be ignored. Assuming

$$\{\Delta\}=\{\phi\}e^{i\omega t}, \tag{124}$$

where $\{\phi\}$ and ω is the mode vector and natural frequency respectively, Eq. (123) leads to the eigenvalue problem

$$\left([K]-\omega^2[M]\right)\{\phi\}=\{0\}, \tag{125}$$

which may be solved by employing different numerical methods[45]. The basic one is the determinant search method in which ω is found from the condition

$$\left|[K]-\omega^2[M]\right|=0 \tag{126}$$

by an iteration procedure. Afterwards, $\{\phi\}$ follows from (125) assuming unit value for one element in $\{\phi\}$.

The forced vibration analysis may be performed by direct integration of Eq. (123), as well as by the modal superposition method. In the latter case the displacement vector is presented in the form

$$\{\Delta\}=[\phi]\{X\}, \tag{127}$$

where $[\phi]=[\{\phi\}]$ is the undamped mode matrix and {*X*} is the generalised displacement vector. Substituting (127) into (123), the modal equation yields

$$[k]\{X\}+[c]\{\dot{X}\}+[m]\{\ddot{X}\}=\{f(t)\}, \tag{128}$$

where

$$\begin{aligned}
&[k] = [\phi]^T [K][\phi] - \text{modal stiffness matrix} \\
&[c] = [\phi]^T [C][\phi] - \text{modal damping matrix} \\
&[m] = [\phi]^T [M][\phi] - \text{modal mass matrix} \\
&\{f(t)\} = [\phi]^T \{F(t)\} - \text{modal load vector.}
\end{aligned} \tag{129}$$

The matrices [k] and [m] are diagonal, while [c] becomes diagonal only in a special case, for instance if [C] = α_0 [M] + β_0 [K], where α_0 and β_0 are coefficients [44].

Solving (128) for undamped natural vibration, [k] = [$\omega^2 m$] is obtained, and by its backward substitution into (128) the final form of the modal equation yields

$$[\omega^2]\{X\} + 2[\omega][\zeta]\{\dot{X}\} + \{\ddot{X}\} = \{\varphi(t)\}, \tag{130}$$

where

$$\begin{aligned}
&[\omega] = \left[\sqrt{\frac{k_{ii}}{m_{ii}}}\right] - \text{natural frequency matrix} \\
&[\zeta] = \left[\frac{c_{ij}}{2\sqrt{(k_{ii} m_{ii})}}\right] - \text{relative damping matrix} \\
&\{\varphi(t)\} = \left\{\frac{f_i(t)}{m_{ii}}\right\} - \text{relative load vector.}
\end{aligned} \tag{131}$$

If [ζ] is diagonal, the matrix Eq. (130) is split into a set of uncoupled modal equations.

The ship vibration is caused by the engine and propeller excitation forces, which are of periodical nature and therefore can be split into harmonics. Thus, the ship's hull response is obtained solving either (123) or (128). In both cases, the system of differential equations is transformed into a system of algebraic equations.

If hull vibration is induced by waves, the time integration of (123) or (128) has to be performed. Several numerical methods are available for this purpose, as for instance the Houbolt, the Newmark and the Wilson θ method, as well as the harmonic acceleration method [46,47].

It is important to point out that all stiffness and mass matrices of the beam finite element (and consequently those of the assembly) are frequency dependent quantities, due to coefficients α and η in the formulation of the shape functions, Eqs.

(107) and (108). That results in the physically consistent natural modes which are not orthogonal and therefore their application in the modal superposition method for forced vibration analysis is not practical, especially not in the case of time integration. Hence, it is preferable to use mathematical orthogonal modes for that purpose. They are created by the static displacement relations yielding from Eqs. (97) and (98) with $\omega = 0$, that leads to $\alpha = \eta = 1$. In that case all finite element matrices, defined with Eqs. (110), can be transformed into explicit form, as shown in [30].

5.5 Numerical example

The application of the improved theory and numerical procedure is illustrated in case of an 11400 TEU VLCS (Very Large Container Ship), Fig. 11. The main vessel particulars are the following:

Length overall	L_{oa} = 363.44 m
Length between perpendiculars	L_{pp} = 348 m
Breadth	B = 45.6 m
Depth	H = 29.74 m
Draught	T = 15.5 m
Displacement, full load	Δ_f = 171445 t
Displacement, ballast	Δ_b = 74977 t
Displacement, light weight	Δ_l = 37151 t
Engine power	P = 72240 kW
Ship speed	v = 24.7 kn

The midship section, which shows a double skin structure with the web frames and longitudinals, is presented in Figure 12. The ship hull stiffness properties are calculated by the program STIFF [48], based on the theory of thin-walled girders, [47]. Their distributions along the ship are shown in [30]. Influence of transverse bulkheads is taken into account by increasing value of torsional modulus $I_t^* = 1.9 I_t$ according to the theory presented in [49]. The lightweight loading condition, i.e. without containers, is considered. Ship mass distribution and its properties are also given in [30].

Dry natural vibrations, as prerogative for hydroelastic analysis, are calculated by the modified and improved program DYANA, [50]. The ship hull is divided into 50 beam finite elements. Ordinary finite elements for closed cross-sections are used for the ship bow, ship aft and in the engine room area.

Natural frequencies of vertical vibrations, and those of coupled horizontal and torsional vibrations are listed in Table 3 and 4 and are compared to the results obtained by 3D FEM analysis. Quite good agreement is achieved for the first few natural modes.

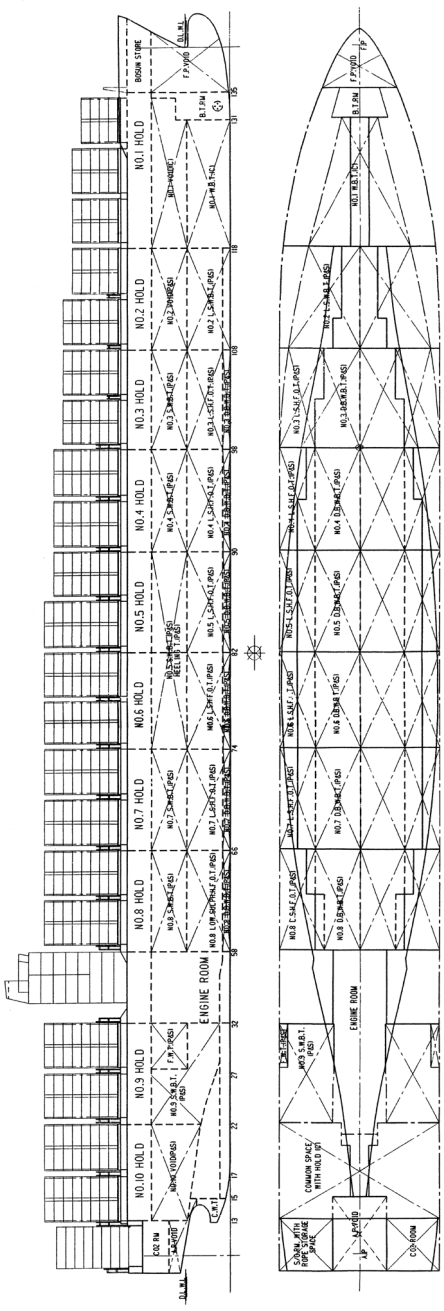

Fig. 11. 11400 TEU container ship

Sl. 11. Kontejnerski brod od 11400 TEU

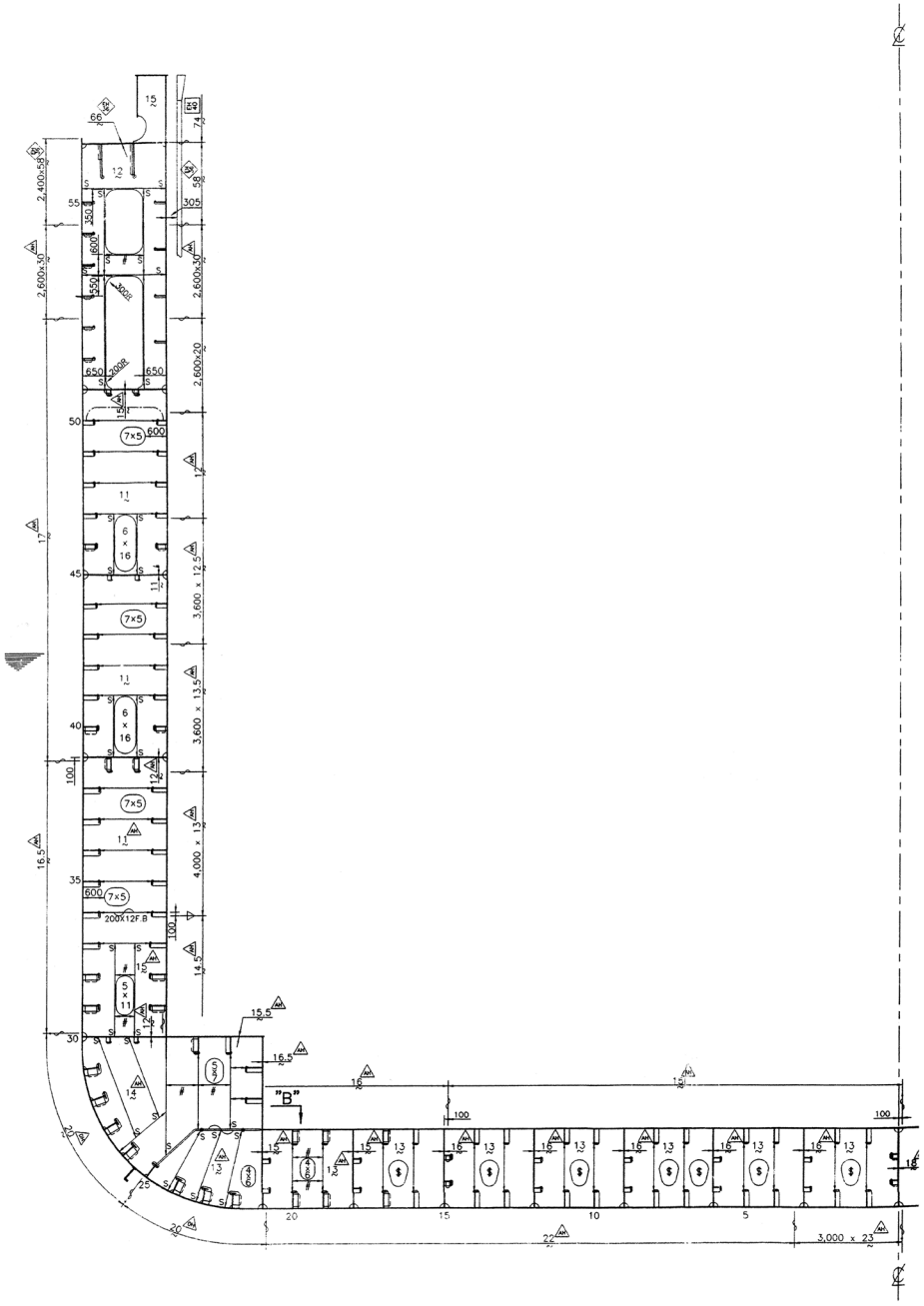

Fig. 12. Midship section

Sl. 12. Poprečni presjek kontejnerskog broda

Table 3 - Natural frequencies of vertical hull vibrations, ω_i (Hz)

Mode no.	1D FEM	3D FEM	Discrepancy %
1	1.149	1.159	-0.86
2	2.318	2.327	-0.39
3	3.695	3.654	1.12
4	5.457	5.409	0.89
5	6.913	6.605	4.66

Table 4 - Natural frequencies of coupled horizontal and torsional hull vibrations, ω_i (Hz)

Mode no.	Coupled modes	1D FEM	3D FEM	Discrepancy %
1	T1	0.639	0.638	0.16
2	T2+H1	1.056	1.076	-1.86
3	T3+H2	1.745	1.749	-0.23
4	T4+H3	2.233	2.429	-8.07
5	T2+H5	3.072	2.630	16.81
6	T5+H4	3.350	3.519	-4.80

Nodal displacements, i.e. translation and rotation of beam model, are transferred to the ship wetted surface. The first natural mode of vertical vibration as well as that of coupled horizontal and torsional vibrations are shown in Figs. 13 and 14, respectively. Also, the later mode determined by the 3D FEM analysis is shown in Fig. 15. 1D and 3D natural mode is of the same shape.

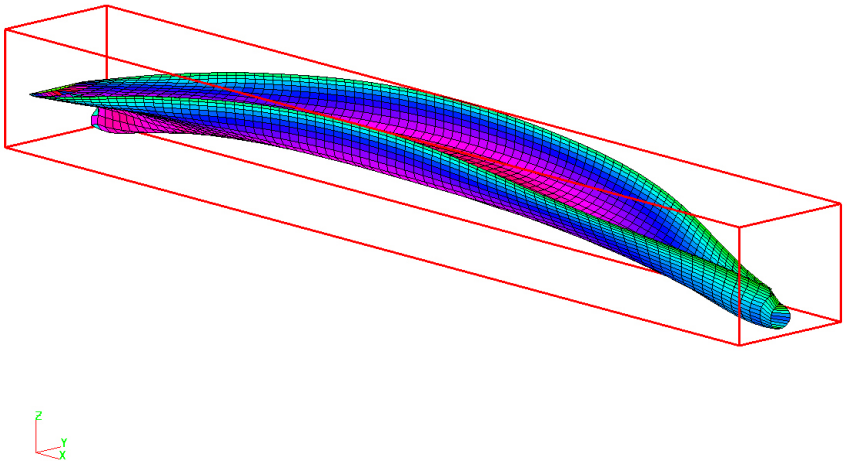

Fig. 13. The first natural mode of vertical vibrations, ω_1=1.149 Hz, 1D model

Sl. 13. Prvi prirodni oblik vertikalnih vibracija, ω_1=1.149 Hz, 1D model

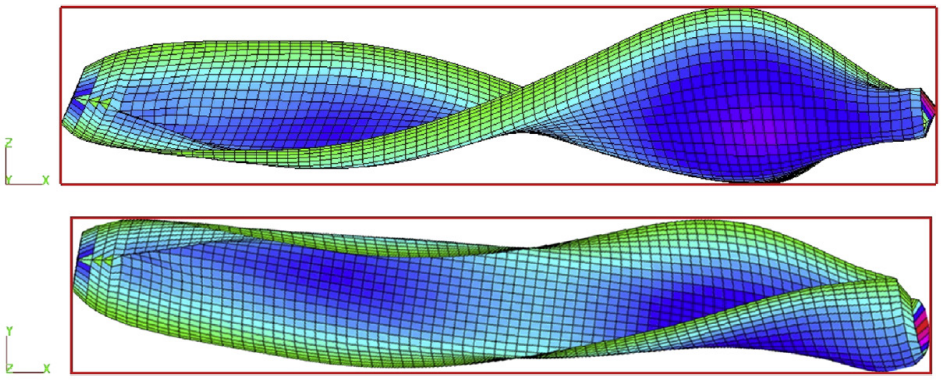

Fig. 14. The first natural mode of coupled horizontal and torsional vibrations, $\omega_1 = 0.639$ Hz, 1D model

Sl. 14. Prvi prirodni oblik spregnutih horizontalnih i torzijskih vibracija, $\omega_1 = 0.639$ Hz, 1D model

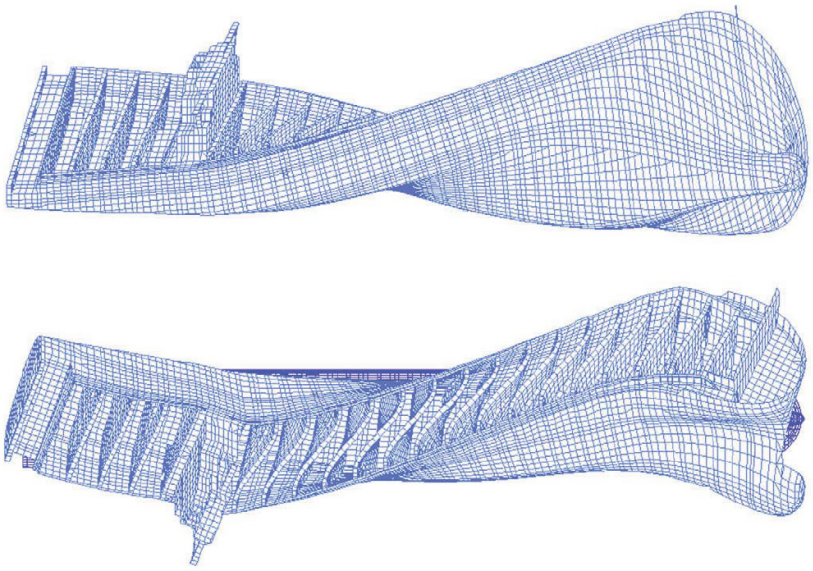

Fig. 15. The first natural mode of coupled horizontal and torsional vibrations, $\omega_1 = 0.638$ Hz, 3D FEM model

Sl. 15. Prvi prirodni oblik spregnutih horizontalnih i torzijskih vibracija, $\omega_1 = 0.638$ Hz, 3D FEM model

6. CONCLUSION

Writing of this paper was motivated by the fact that Timoshenko beam theory after 93 years is still actual. As pointed out in Introduction it has been used at the beginning for dynamic analysis of structural elements, and later on for structural analysis of bridges. Nowadays, its application is extended to large range of scale, from nanotubes to ultra large structures.

The paper is dealing with two presently interesting subjects, i.e. dynamic behavior of nanotube embedded in an elastic medium and exposed to moving nanoparticle gravity load, and vibrations of ultra large container ships. In both cases the modified Timoshenko beam theory is used, which results with simpler problem formulations. Nanotube response is determined semi-analytically and parametric analysis is performed emphasizing influence of damping on response.

Even complex structures like ultra large container ships can be modeled as a beam for global response analysis if flexural and torsional stiffness parameters of ship cross-section are determined in a sophisticated way by the advanced thin-walled girder theory and if influence of transverse bulkheads and relatively short engine room structure are taken into account in a proper way. Dry natural vibrations are prerogative for hydroelastic analysis of ship exposed to wave excitation by the modal superposition method. Such an analysis includes also determination of modal restoring stiffness, added mass and damping. Correlation of natural eigenpairs (frequency and modes) determined by the beam model with those obtained by 3D FEM model shows high reliability of the former.

Timoshenko beam theory is only one topic worked out by that genius scientist, but unique one due to long time and broad application. Probably, he could not imagine that application of his beam theory does not end with structural analysis of bridges.

Acknowledgement

The presented investigation has been carried out within the national project of the Croatian Ministry of Science, Education and Sport entitled Load and Response of Ship Structures, the EU FP7 Project TULCS (Tools for Ultra Large Container Ships), and the project Technology for onboard equipment – induced underwater radiated noise analysis and evaluation supported by the National Research Foundation of Korea (NRF) grant founded by the Korean Government (MEST) through GCRG-SOP (Grant no. 2011-0030669).

References

[1] Pilkey WD. Analysis and Design of Elastic Beams, John Wiley & Sons Inc., New York, NY, USA, 2002.
[2] Pavazza R. Introduction to the Analysis of Thin-Walled Beams, Kigen, Zagreb, Croatia. (in Croatian), 2007.
[3] Carrera E, Giunto G, Petrolo M. Beam Structures, Classical and advanced Theories, John Wiley & Sons Inc., New York, NY, USA, 2011.
[4] Timoshenko SP. On the correction for shear of the differential equation for transverse vibration of prismatic bars, Phylosoph. Magazine, **41**(6), 1921, pp. 744-746.
[5] Timoshenko SP. On the transverse vibrations of bars of uniform cross section, Phylosoph. Magazine, **43**, 1922, pp. 125-131.
[6] Timoshenko SP. Vibration Problems in Engineering, 2nd ed., D. van Nostrand Company, Inc. New York, NY, USA, 1937.
[7] Inman DJ. Engineering Vibration, Prentice Hall, Inc., Englewood Cliffs, New Jersey, 1994.
[8] van Rensburg NFJ, van der Merve AJ. Natural frequencies and modes of a Timoshenko beam, Wave Motion, 44, 2006, pp. 58-69.
[9] Geist B, McLaughlin JR. Double eigenvalues for the uniform Timoshenko beam, Appl. Math. Letters, 10(3), 1997, pp. 129-134.
[10] De Rosa MA. Free vibrations of Timoshenko beams on two-parametric elastic foundation, Comput. Struct., 57, 1995, pp. 151-156.
[11] Matsunaga H. Vibration and buckling of deep beam-columns on two-parameter elastic foundations, J. Sound Vibr., 228, 1999, pp. 359-376.
[12] Stojanović V, Kozić P. Forced transverse vibration of Rayleigh and Timoshenko double-beam system with effect of compressive axial load, Intl. J. Mech. Sci., 60, 2012, pp. 59-71.
[13] Stojanović V, Kozić P, Janevski G. Exact closed-form solutions for the natural frequencies and stability of elastically connected multiple beam system using Timoshenko and higher-order shear deformation theory, J. Sound Vibr., 332, 2013, pp. 563-576.
[14] Timoshenko SP. On the forced vibrations of bridges, Philosophical Magazine Series 6, 43, 1922, pp.1018.
[15] Frýba L. Dynamics of Railway Bridges, Thomas Telford Science Ltd., Prague, 1996.
[16] Sniady P. Dynamic response of Timoshenko beam to a moving force, Journal of Applied Mechanics, 75(2), 2008, pp. 0245031-0245034.

[17] Bayer CI, Dyniewicz B. Numerical Analysis of Vibrations of Structures and Moving Inertial Load, Springer-Verlag Berlin Heidelberg, 2012.
[18] Simsek M. Forced vibration of an embedded single-walled carbon nanotube traversed by a moving load using nonlocal Timoshenko beam theory, Steel and Composite Structures, Vol. 11, No. 1, 2011, pp. 59-76.
[19] Kiani K, Wang Q, On the interaction of a single-walled carbon nanotube with moving nanoparticle using nonlocal Rayleigh, Timoshenko, and higher-order beam theories, European Journal of Mechanics A/Solids 31, 2012, pp. 179-202.
[20] Kiani K, Mehri B. Assessment of nanotube structure under a moving nanoparticle using nonlocal beam theories, Journal of Sound and Vibration 329, 2010, pp. 2241-2264.
[21] Aydogdu M. A general nonlocal beam theory: Its application to nanotube bending, buckling and vibration, Physica E 41, 2009, pp. 1651-1655.
[22] Mindlin RD. Influence of rotary inertia and shear on flexural motions of isotropic elastic plates, J. Appl. Mech., 18(1), 1951, pp. 31-28.
[23] Senjanović I, Vladimir N, Tomić M. An advanced theory of moderately thick plate vibrations, Journal of Sound and Vibration 332, 2013, pp. 1868-1880.
[24] Zhou D. Vibrations of Mindlin rectangular plates with elastically restrained edges using static Timoshenko beam functions with Rayleigh-Ritz method, Intl. J. Solids Struct., 38, 2001, pp. 5565-5580.
[25] Pavazza R. Torsion of thin-walled beams of open cross-sections with influence of shear, Intl. J. Mech. Sci., 47, 2005, pp. 1099-1122.
[26] Reddy JN. On locking free shear deformable beam elements, Comput. Meth. Appl. Mech. Eng., 149, 1997, pp. 113-132.
[27] Senjanović I, Tomić M, Hadžić N. Moving load and beam response: A systematic investigation and analytical solution of Timoshenko beam vibrations excited by moving gravity and inertia force, LAP LAMBERT Academic Publishing, Saarbrücken, Germany, 2014.
[28] Senjanović I, Vladimir N. Physical insight into Timoshenko beam theory and its modification with extension, Structural Engineering and Mechanics, Vol. 48, No. 4, 2013, pp. 519-545.
[29] Senjanović I, Tomić M, Hadžić N. Nonlocal vibrations of a carbon nanotube due to moving nanoparticle gravity and inertia force determined semi-analytically by the modified Timoshenko beam theory, Journal of the Mechanical Behavior of Materials, 23, 2014, pp. 109-128.
[30] Senjanović I, Tomašević S, Vladimir N. An advanced theory of thin-walled girders with application to ship structures, Marine Structures 22, 2009, pp. 387- 437.

[31] Cowper GR. The shear coefficient in Timoshenko's beam theory, J. Appl. Mech., 33, 1966, pp. 335-340.
[32] Senjanović I, Fan Y. A higher-order flexural beam theory, Comput. Struct., 10, 1989, pp. 973-986.
[33] Li XF. A unified approach for analysing static and dynamic behaviours of functionally graded Timoshenko and Euler-Bernoulli beams, J. Sound Vibr., 32(5), 2008, pp. 1210-1229.
[34] Thomson WT. Theory of Vibration with Applications, George Allen & Unwin, London, 1981.
[35] Zhou X, Shin E, Wang KW, Bakis CE. Interfacial damping characteristics of carbon nanotube-based composites, Composite Science and Technology, 64, 2004, pp. 2425-2437.
[36] Bishop RED, Price WG. Hydroelasticity of Ships. Cambridge University Press; 1979.
[37] Senjanović I, Malenica Š, Tomašević S, Rudan S. Methodology of ship hydroelasticity investigation. Brodogradnja, 58(2), 2007, pp. 133-45.
[38] Senjanović I, Malenica Š, Tomašević S. Investigation of ship hydroelasticity. Ocean Engineering 35, 2008, pp. 523-535.
[39] Kawai T. The application of finite element methods to ship structures. Computers & Structures, 3, 1973, pp. 1175-1194.
[40] Senjanović I, Grubišić R. Coupled horizontal and torsional vibration of a ship hull with large hatch openings, Computers & Structures 41(2), 1991, pp. 213-226.
[41] Wu JS, Ho CS. Analysis of wave induced horizontal- and torsion coupled vibrations of ship hull, Journal of Ship Research, 31(4), 1987, pp. 235-252.
[42] Pedersen PT. Torsional response of container ships, Journal of Ship Research 29, 1985, pp. 194-205.
[43] Pavazza R. Bending and torsion of thin-walled beams of open section on elastic foundation, Ph.D. Thesis, University of Zagreb, 1991 (in Croatian).
[44] Senjanović I. Ship Vibrations, Part 2, textbook. Zagreb: University of Zagreb, 1990.
[45] Bathe KJ. Finite element procedures. Englewood Cliffs, NJ: Prentice-Hall; 1996.
[46] Senjanović I. Harmonic acceleration method for dynamic structural analysis. Computers & Structures 18(1), 1984, pp. 71-80.
[47] Lozina Ž. A comparison of harmonic acceleration method with the other commonly used methods for calculation of dynamic transient response. Computers & Structures, 29(2), 1988, pp. 227-240.
[48] Fan Y, Senjanović I. STIFF, User's manual. Faculty of Mechanical Engineering and Naval Architecture, Zagreb, 1990.

[49] Senjanović I, Tomašević S, Rudan S, Senjanović T. Role of transverse bulkheads in hull stiffness of large container ships. Engineering Structures 30, 2008, pp. 2492-2509.

[50] Čorić V, Augustinović T, Senjanović I, Fan Y. DYANA, User's Manual, Faculty of Mechanical Engineering and Naval Architecture, Zagreb, 1989.

Timošenkova teorija grede nakon 93 godine – preko mostova do nanocijevi i ultra velikih brodova

Sažetak

Sažeto je prikazana Timošenkova teorija grede, koja operira s progibom i kutom zakreta poprečnog presjeka kao osnovnim varijablama. Teorija je nadalje modificirana raspr ežući ukupni progib grede u progib čistog savijanja i progib uslijed smika, te ukupni kut zakreta u kut uslijed savijanja i kut uslijed uzdužnog smicanja. Osnovne jednadžbe su spregnute u dvije nezavisne jednadžbe gibanja, jedna za savojne, a druga za uzdužne smične vibracije. Jednadžbe su rješene za slučaj prirodnih vibracija. Razmatran je problem vibracija nanocijevi u elastičnom mediju uvođenjem parametara nelokalnog naprezanja. Parcijalna diferencijalna jednadžba 4-tog reda za savojne vibracije proširena je na jednadžbu 6-tog reda. Odziv nanocijevi na pomičnu gravitacijsku silu nanočestice analiziran je koristeći metodu superpozicije prirodnih oblika vibriranja, metodu separacije varijabli, Galerkinovu metodu i metodu ravnoteže harmonika. U nastavku razmotren je problem spregnutih savojnih i torzijskih vibracija tankostijenog nosača. Korištena je modificirana Timošenkova teorija grede za savojne vibracije. Složeni problem torzijskih vibracija uz vitoperenje poprečnog presjeka nosača formuiliran je na analogan način. Za potrebe analize vibracija neprizmatičnog brodskog trupa razvijen je sofisticirani gredni konačni element. Primjena razvijenih teorija ilustrirana je na primjerima analize vibracija nanocijevi i jednog ultra velikog kontejnerskog broda.

Ključne riječi: Timošenkova teorije grede; nanocijev; pomično opterećenje; tankostijeni nosač; savojne vibracije; torzijske vibracije; kontejnerski brod

Ivo Senjanović
University of Zagreb
Faculty of Mechanical Engineering
and Naval Architecture
Ivana Lučića 5, 10000 Zagreb
Croatia
e-mail: ivo.senjanovic@fsb.hr

Nikola Vladimir
University of Zagreb
Faculty of Mechanical Engineering
and Naval Architecture
Ivana Lučića 5, 10000 Zagreb
Croatia

Marko Tomić
University of Zagreb
Faculty of Mechanical Engineering
and Naval Architecture
Ivana Lučića 5, 10000 Zagreb
Croatia

Neven Hadžić
University of Zagreb
Faculty of Mechanical Engineering
and Naval Architecture
Ivana Lučića 5, 10000 Zagreb
Croatia

UDK / UDC 629.5
Izvorni znanstveni članak / Orginal scientific paper
Prihvaćeno / Accepted: 19. 2. 2015.

PROCEDURE FOR THE SERVICE STRENGTH APPROVAL OF THE DRILLSHIP DERRICK

Vatroslav V. Grubišić and Jani Barle

Abstract

Service strength approval of a drillship derrick must include beside the static strength validation under limit loads, also the fatigue evaluation for the critical areas of the derrick structure. During the service life structural members of the derrick are exposed to giga stress cycles with variable values, caused by wave and wind action and drilling operation. These variable stresses can generate the fatigue cracks and lead to the total fracture of the structure. For the fatigue strength evaluation of a drillship derrick is important to define the loading taking into account the drillship usage. To determine the loading it is necessary to evaluate the ship motion and to calculate the corresponding loads due to waves, wind and drilling operation acting on the derrick structure. For the fatigue life validation, the resulting stresses, caused by these loads must be determined and their representative spectra (cumulative frequency distributions) derived.

In this paper the procedure to determine the operational stress spectra and to evaluate the fatigue life of a drillship derrick is described.

Keywords: Operational loading; Stress spectra; Drillship derrick; Service strength; Fatigue life estimation

1. INTRODUCTION

Due to development in energy market the number of drill ships (Fig.1) in the offshore drilling fleet has been more than doubled over the past decade, from 37 operating units in 2003 to 87 units in 2013. Further growth is expected over the next years developing drillship systems with higher efficiency and usage at higher drilling depth, polar temperatures and harsh environmental conditions.

The service strength validation of a drillship derrick must include as well the **static strength control**, based on nominal stresses in individual cross sections of the structure (failure criterion: **buckling** ;requirement: maximum monotonic stress lower than the structural yield point) and the **fatigue evaluation** for the critical areas of

the derricks structure, based on local hot-spot stress (failure criterion: **fatigue cracks**; requirement: cyclic stresses under variable service loading lower than the allowable stress) for the specific service stress spectrum.

Figure 1. Drillship with derrick

Slika 1. Brod za podmorska bušenja s bušaćim tornjem.

During the service life structural members of derrick are exposed to more than 10^8 stress cycles with variable amplitudes, caused by wave and wind action and drilling operation, which can generate the fatigue cracks, as shown on an example in Fig.2, and lead to a total fracture of the derrick.

Figure 2.Cracks on derrick footing after 20 years usage.

Slika 2. Naprsline na nogama tornja nakon 20 godina upotrebe.

For the fatigue strength evaluation of a drillship derrick it is important to define the loading taking into account the drillship usage. To determine the loading it is necessary to evaluate the ship motion and to calculate the respective loads acting on the derrick structure due to waves, wind and drilling operation. Finally the resulting stresses, caused by these loads must be determined and their representative spectra (cumulative frequency distributions) derived to be used for the fatigue life validation. For the fatigue validation of a drillship derrick it is of paramount importance to determine the representative service stress spectra for possibly critical, fatigue sensitive, system-points of the structure. Due to a very complex loading at operation, caused by ship motion and wind blowing with changing direction and intensity (speed), reliable praxis related service stress spectra should be used for the fatigue validation.

Beside the stress spectra also the fatigue strength, to be used for fatigue validation, is of decisive importance. Predominantly the critical system-points are welds on which, on one side the stress concentration is present and on other side the fatigue strength is lower than in non-welded areas. Also the bolted connections could be critical and should be in such a case approved using the corresponding stress spectra.

In this paper the methodology to evaluate the fatigue life [1] of a drillship derrick is described.

Prerequisites to validation described in this paper are: (a) approval of the static strength including buckling evaluation of structural members under monotonic extreme loading and (b) check of the local hot-spot stresses in individual areas of the derrick with respect to the structural yield point. At the design process the allowable maximum local (structural or hot-spot) stress can be determined by a conservative simplified approach based on material yield point $R_{p,0.2}$ taking into account the required safety factor S_F (usually 1.15) : $\sigma_{max,all} \leq (0.9\, R_{p,0.2} + 0.002\, E) / S_F$.

2. SERVICE STRESS SPECTRA

The service stress spectra valid for specific area (system point of the derrick) are defined by the **spectrum maximum value** $\Delta\sigma_0$, the **spectrum shape** h and the **number of cycles** n_0 for the required fatigue life. The probability of occurrence of the specific stress spectrum must be defined additionally, to be able to carry out a reliable fatigue validation. The stress spectrum can be presented [2,3] by two-parameter Weibull cumulative frequency distribution of stress range of exceedances $Q(\Delta\sigma)$. The $Q(\Delta\sigma)$ correspond to the probability that a value exceeds $\Delta\sigma$.

$$Q(\Delta\sigma) = \frac{n(\Delta\sigma)}{n_0} = \exp\left[-\left(\Delta\sigma / q\right)^h\right] \tag{1}$$

where: h – Weibull shape parameter; n_0 – number of cycles over the time period for which the stress range level $\Delta\sigma_0$ is defined; $\Delta\sigma_0$ – the largest stress range corresponding to n_0 cycles from the load spectrum and q – Weibull scale parameter defined from the stress range level $\Delta\sigma_0$ as $=\Delta\sigma_0 (ln\ n_o)^{-1/h}$.

A schematic presentation of the stress spectra is given in Figure 3.

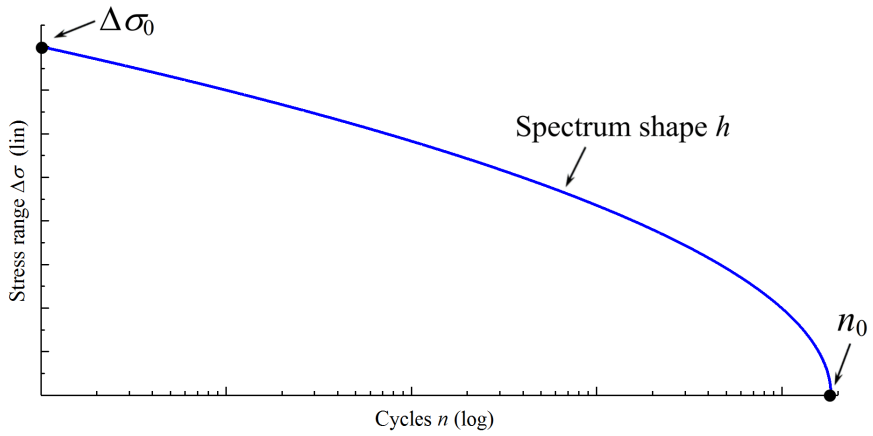

Figure 3. Schematic presentation of service stress spectrum.
Slika 3. Shematski prikaz spektra pogonskog opterećenja.

The stress range contains stress maximum and the stress minimum for specific lading defining the stress ratio between the minimum to maximum value of the stress in a cycle.

2.1 Operational stresses

The loads acting on derrick are result of ship motion (heave, roll, pitch) due to **waves**, **wind** activity and **drilling** operation. These loads generate variable stresses in individual system-points of derrick. To systemize these stresses the loading due to the ship motion in waves is divided in operational conditions at **navigation** and at **drilling**.

Navigation (NA) include different loading conditions: survival loading with 25 m wave height and wind up to 52 m/s speed, navigation at "bad weather" with waves of 15-25 m height and wind up to 52 m/s speed, navigation at "rough sea" with waves of 6m and wind of 16 m/s and navigation at calm weather condition, with specific usage time and loading resulting in different stress spectra.

Drilling (DR) operation could be divided in drilling at moderate/high sea state and wind up 17 m/s, and drilling with overpool at low ship motion with waves up to 4 m and wind up to 17 m/s.

The largest service stress range $\Delta\sigma_{0,i}$ for individual spectrum is determined based on acting loads and the stress calculation of derricks structure. The maximum values for ship motion and environmental loading at navigation are chosen to be extreme loading condition for stress spectrum which is used also for the static strength validation. The ship motion and environmental condition values for the load case NA are chosen to be extreme environmental condition according to the maximal load forces values for survival conditions which is used also for the static strength validation

2.2 Spectrum shape

Beside the stress $\Delta\sigma_{0,i}$ the shape parameter h in the Weibull distribution has a significant impact on calculated fatigue damage. Taking into account the data in literature and recommendations [4-6] a shape parameter for the service stress spectrum generated through environmental loading (wind and waves) between $h = 0.8$ and $h = 1.1$ should be used. It is proposed to use value $h = 1$ for the resulting spectrum and spectra for the environmental loading at drilling. For the spectrum of drilling operations value $h = 1.1$ to 1.2 is proposed.

2.3 Number of cycles

The number of cycles $\boldsymbol{n_0}$ for individual usage depends on the dynamic behavior of the structure under the specific loading. The dynamic response of the derrick structure to the environmental loading (wind and waves) depends on its natural frequencies ν_0.

For the spectra at drilling the maximal load up-crossing frequency is determined by the ship motion which is usually lower than the natural frequency of the derrick.

The number of cycles per year (n_0 / y) for each loading case is achieved by multiplying the time spent in seconds with specified frequency ν_0 (n_0 / y = days · 24 · 3.6·1 0^3· ν_0).

Based on a natural frequency ν_0 of derrick and a ship usage of 25 days per year at **navigation** the number of cycle per year due to the navigation NA will result in a value of about $2.16 \cdot 10^6$ cycles.

Due to the requirements for the fatigue validation the spectrum at **drilling** is divided in two partial spectra, one for the drilling including the environmental loading (DR+E) with the frequency of ship motion ν_0 =0.1 Hz and the second for the environmental loading at drilling alone (E) with natural frequency ν_0 =1.0 Hz. The number

of cycles at drilling DR+E results from cycles at drilling per each well and number of wells per year. Assuming a value for 4. $6 \cdot 10^3$ cycles per each well and four wells per year it results in $1.84 \cdot 10^4$ cycles for this load case. Based on a time of 310 days at drilling operation the number of cycles for the superimposed environmental loading alone will result in a value of roughly $2.68 \cdot 10^6$ cycles per year. The resulting total number of· $3.6 \cdot 10^3$ cycles per year will be then about $n_0 / y = 4.86 \cdot 10^3$ and in the case of 30 years usage about $1.46 \cdot 10^8$ cycles

3. FATIGUE VALIDATION

The fatigue validation must be carried out for individual, highly stressed, possibly critical, system points of the derrick. As an example the system points of a derrick are shown in Fig.4, which must be controlled concerning fatigue under expected service loading.

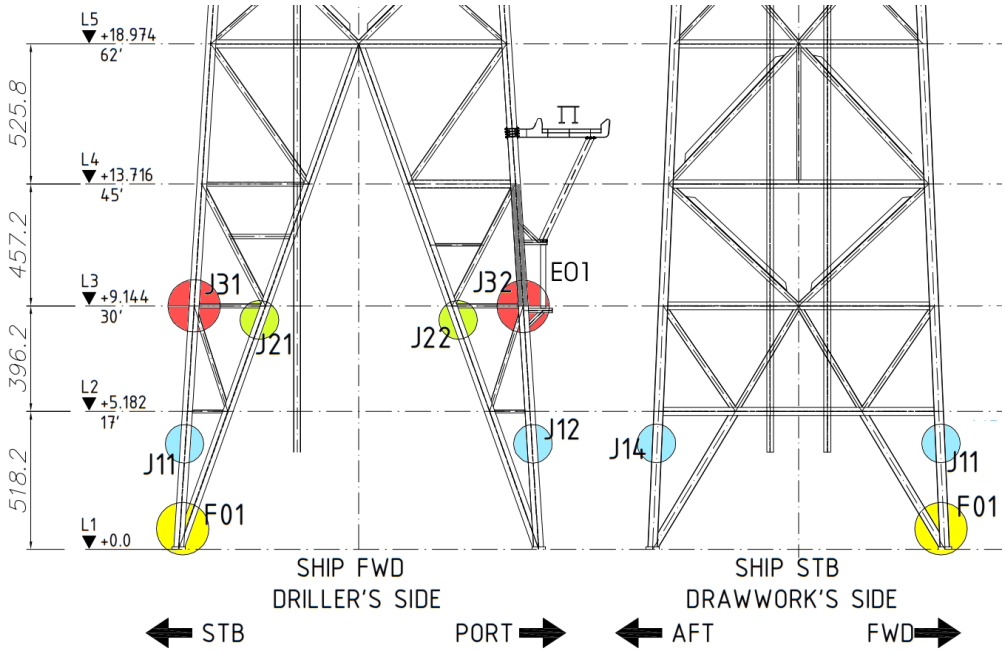

Figure 4. Possibly critical system points of a derrick to be validated respective fatigue.

Slika 4. Moguća kritična mjesta na bušaćem tornju na kojima treba provesti provjeru čvrstoće na zamor.

The fatigue validation must include the representative stress spectrum for each possibly critical system point of the derrick and the corresponding fatigue strength. For the fatigue validation following stresses, based on calculation, are used:

- prestress due to the weight σ_{DW},
- maximum calculated stress σ_{max}, which contains as well the prestress as the stress generated by the drilling and the environmental loading, as used for the static validation of the structure,
- maximum value for the superimposed environmental loading σ_E due to the ship motion and wind action,
- extrapolated stress for fatigue validation at navigation $\Delta\sigma_E$ ($\Delta\sigma_E = \sigma_{max} - \sigma_{DW}$) and
- extrapolated stress for fatigue validation at drilling $\Delta\sigma_E = 1.5 \cdot \sigma_E$ for environmental loading at drilling alone and $\Delta\sigma_{DR+E}$ ($\Delta\sigma_{DR+E} = \sigma_{max} - \sigma_{DW} = \Delta\sigma_{DR} + \sigma_E$) for drilling including superimposed environmental loading σ_E

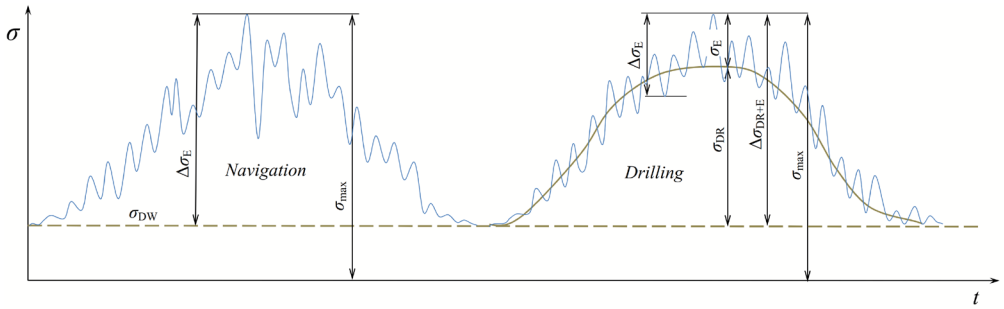

Figure 5. Definition of stress values on a system point which are used for fatigue validation (schematic).

Slika 5. Definicija vrijednosti naprezanja na pojedinom mjestu tornja, koja se koriste za provjeru pogonske čvrstoće (shematski).

The stress values used for fatigue validation must be based on drillship usage, and should correspond to a conservative approach by the assumed combination of extreme loading condition as well with regard to the stress values as to the number of cycles and shape of the specific stress spectrum.

In Fig.6 the stress spectra for individual loading case and a Woehler curve, used for fatigue validation, are presented in stress (σ)-cycles (n) diagram.

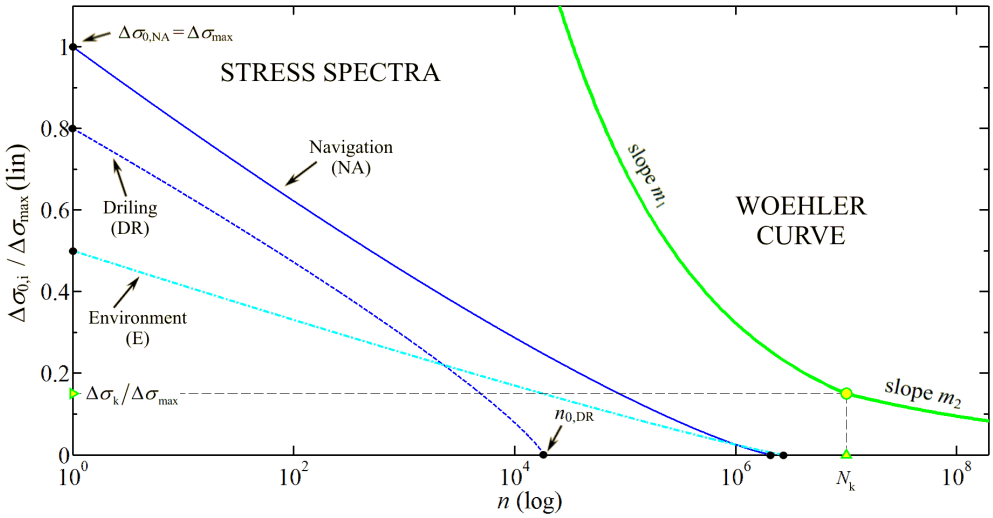

Figure 6. Stress spectra and Woehler curve for fatigue validation

Slika 6. Spektri naprezanja i Woehlerova krivulja za provjeru zamorne čvrstoće.

The fatigue life estimation is made according to the modified Palmgren-Miner damage accumulation hypothesis [1], since the fatigue strength of structures in service is continuously decreasing at high number of stress cycles. The Woehler curve is in this case presented in the stress-cycles diagram as a bilinear curve,Fig. 6; N_k represents the number of cycles at so called 'endurance limit' (knee point of the Woehler curve) having the value for the fatigue validation of welded structures usually $N_k = 10^7$ cycles.

For the bi-linear or two-slope Whoeler curve, as noted in [3, Appendix], the fatigue damage can be calculated by

$$D = n_0 \left[\frac{q^{m_1}}{a_1} \Gamma\left(\frac{m_1}{h} + 1; \left(\frac{\Delta\sigma_k}{q} \right)^h \right) + \frac{q^{m_2}}{a_2} \gamma\left(\frac{m_2}{h} + 1; \left(\frac{\Delta\sigma_k}{q} \right)^h \right) \right] \tag{2}$$

where: $\Delta\sigma_k$– stress range for which change of slope of Woehler curve occur; N_k– number of cycles for which change of slope of Woehler curve occur; $\Gamma(\alpha\ ;\ x)$– the complementary incomplete gamma function; $\gamma(\alpha\ ;\ x)$– the incomplete gamma function; m– negative inverse slope of the Woehler curve; ā intercept of the design Woehler curve with the log N axis; $\bar{a}_1$, m_1– Woehler curve fatigue parameters ($\bar{a}_1 = N_k \cdot \Delta\sigma_k^{m_1}$) for $\Delta\sigma > \Delta\sigma_k$; $\bar{a}_2$, m_2– Woehler curve fatigue parameters ($\bar{a}_2 = N_k \cdot \Delta\sigma_k^{m_2}$) for $\Delta\sigma \leq \Delta\sigma_k$.

The calculated fatigue damage D must be lower than the allowable value: $D_{calc} \leq D_{all} \leq 1$. Nevertheless of the modifications related to the calculation of damage accumulation by Palmgren-Miner hypothesis , the investigations and practical experience revealed damage values different from the theoretical value $D = 1$, depending on stress-time history, stress distribution and material behaviour. Therefore a damage sum of $D_{all} = 0.5$ is recommended for welded structures [1,3,5-8].

In order to perform a reliable validation, the scatter of the fatigue strength as the service loading spectra, must also be taken into account. Therefore, the service load spectra represent the extreme usage condition (that means that probability of occurrence of this spectrum will be very low $P_o \leq 1\%$) and the Woehler curve has a high probability of survival $P_s \geq 90$ %, so that the resulting probability of failure for the durability life will be low ($P_f \leq 0.1\%$.) if the calculated damage is $D \leq 0.5$.

The fatigue damage D should be calculated for the stress spectrum of each load case. Hence it will be possible to determine which load case is decisive for the fatigue strength of the specific derrick area.

The fatigue validation is influenced, beside of the service stress spectra, decisively from the structural fatigue properties for each critical system point of the derrick. For the welded structural details, being usually the critical points, the data for Woehler curves can be found in specific codes and norms [5,7,8]. Also bolted connections in highly stressed areas should be validated using specific data [5]. In specific cases also the influence of a low temperature at drillship usage or corrosion should be taken into account.

As an example for the described procedure a welded structural detail of the derrick the system point J 32, Fig. 4 is analysed. This structural detail correspond to detail category C1 , Ref. [4], with calculated maximum values of the stresses for loading case: $\Delta\sigma_0 = 320$ MPa at navigation, $\Delta\sigma_0 = 250$ MPa at drilling with superimposed environmental loading and $\Delta\sigma_0 = 220$ MPa due to the environmental loading alone.

The data used for the fatigue validation and results for individual loading case are summarized in Table 1. The Woehler curve are based on Ref. [5] with following data: for the fatigue strength $\Delta\sigma_k = 65.5$ MPa at $N_k = 10^7$ cycles and slopes of Woehler curve $m_1 = 3$ and $m_2 = 5$.

Specific data related to the stress spectra for individual loading condition per year and Woehler curve, used for calculation of fatigue damage are presented in Fig. 7.

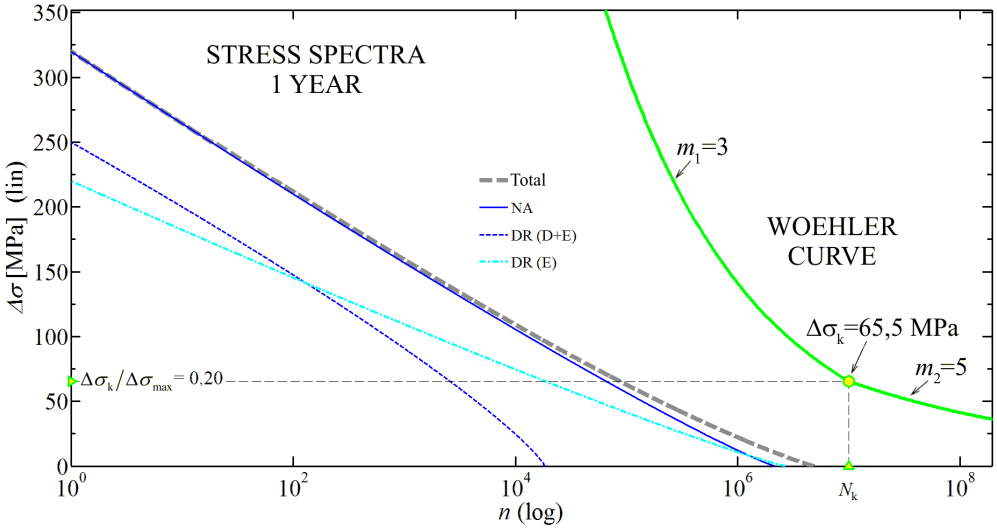

Figure 7 Stress spectra for one year and Woehler curve used for fatigue validation.

Slika 7. Spektri pogonskih naprezanja za jednu godinu i Woehlerova krivulja za provjeru pogonske čvrstoće.

The results of the calculation are summarized in Table 1:

Table 1. The data for the fatigue damage calculation and resulting fatigue life estimation.

Tablica 1. Ulazne vrijednosti za proračun oštećenja i odgovarajuća procjena životnog vijeka.

$\Delta\sigma_k$ = 65,50 MPa; $N_k = 10^7$; m_1= 3; m_1= 5 Raturn period : 1 Year					
FLC	$\Delta\sigma_{0,i}$ (MPa)	$n_{0,i}$	h_i	D_i	%
NA	320,00	2.16E+06	0,9	2,47E-02	75,0%
DR (D+E)	250,00	1.84E+04	1,2	1,03E-03	3,1%
DR (E)	220,00	2.68E+06	0,9	7,22E-03	21,9%
Per Y =		4,86E+06		3,30E-02	
Estimated life : $D_{all} / \sum D_i$ = 0,5 / 0,033 = 15,15 Years					

The expected fatigue life with respect to the criteria of an initial crack based on this calculation is about 15years.To assure a higher fatigue life an improvement in this area would be necessary. From the Table 1 it can be seen that 75% of the fatigue dam-

age is generated by the stress spectra due to the navigation and 25% by the loading case of drilling, mainly due to the superimposed environmental loading at drilling.

4. CONCLUSION

For the fatigue validation of a drillship derrick it is of paramount importance to determine the representative service stress spectra for possibly critical, fatigue sensitive, system-points of the structure. Due to a very complex loading during operation, caused by ship motion in waves and wind blowing with changing direction and intensity (speed), reliable praxis related service stress spectra should be used for the fatigue validation.

Beside the stress spectra also the fatigue strength, to be used for fatigue validation, is of decisive importance. Predominantly the critical system-points are welds on which, on one side the stress concentration is present and on other side the fatigue strength is lower than in non-welded areas. Also the bolted connections could be critical and should be in such a case approved using the corresponding stress spectra.

It is proposed to verify the data used to derive the service stress spectra by service measurements, at which the stress time histories on selected system-points of the derrick should be determined in correlation to the wave and wind intensities.

It is also important that beside the described fatigue strength validation, during the usual periodical ship inspections the highly stressed system points of the derrick, determined at validation, are controlled regarding possible initial cracks.

Acknowledgment

This paper is prepared with support of the Company GOE-"Global Offshore Engineering", Split, which allowed to use the data from a project related to the reconstruction of an used drillship derrick and is based on requirements for the fatigue validation of DNV- " Det Norske Veritas" , Ref. [2,5,6]

REFERENCES

[1] Grubišić, V.: Development of Structural Durability Validation-from Woehler's Endurance Limit to the Durability of the Axles of Modern Trains. Croatian Academy of Sciences and Arts, Zagreb. Department of Technical Sciences, Bulletin No.1 (2007), pp. 1-27.

[2] DNV-RP-C205, 2010: Environmental conditions and environmental loads

[3] Barle, J.; Grubišić,V.; Radica, D.: Service strength validation of wind-sensitive structures, including fatigue life evaluation. Engineering Structures. 32(9), 2010, pp. 2767–2775.

[4] Schuetz, W.; Klaetschke, H.; Hueck, M.;Sonsino, C.M.: Standardized Load Sequence for Offshore Structures -WASH 1; Fatigue Fract. Engng. Mater. Struct. Vol. 13, No.1, pp.19-29, 1990 .

[5] DNV-RP-C203, 2010: Fatigue strength analysis of offshore steel structure.

[6] DNV-CN30.7, 2010: Fatigue assessment of ship structures.

[7] ISO 12110-1:2013: Metallic materials - Fatigue testing - Variable amplitude fatigue testing - Part 1: General principles, test method and reporting requirements.

[8] European Committee for Standardization (CEN), Eurocode 3: Design of steel structures Part 1-9: Fatigue EN 1993-1-9:2005, Brussels: CEN; 2005.

Postupak provjere pogonske čvrstoce tornja broda za podmorska bušenja

Sažetak

Provjera pogonske čvrstoće tornja broda za podmorska bušenja mora pored kontrole statičke čvrstoće pod maksimalnim opterećenjem, da sadrži također kontrolu čvrstoće na zamor pojedinih ,kritičnih mjesta strukture tornja. Ta mjesta strukture su opterećena promjenljivim naprezanjima nastalih djelovanjem valova,vjetra i bušenjem pri upotrebi broda sa brojem promjena u giga području. Usljed tih naprezanja mogu nastati zamorne naprsline a njihovo širenje uzrokovati lom čitave konstrukcije. Da bi se mogla izvršiti provjera čvrstoće na zamor, mora se definirati pogonsko naprezanje uzimajući u obzir upotrebu broda. Pri određivanju naprezanja potrebno je analizirati gibanje broda pri pogonskim opterećenjima i odrediti sile koje djeluju na strukturu tornja usljed valova, vjetra i bušenja. Za provjeru čvrstoće na zamor potrebno je odrediti naprezanja uzrokovana tim silama i njihov reprezentativni spektar (raspodjelu zbirne učestalosti naprezanja).

U ovom članku je prikazan postupak za određivanje spektra pogonskih opterećenja i provjeru životnog vijeka bušaćeg tornja broda za podmorska bušenja.

Ključne riječi: Radna opterećenja; Spektar opterećenja; Toranj broda za bušenje; Procjena životnog vijeka na zamor

Vatroslav V. Grubišić
Corresponding member of HAZU; retired head of "Department for Stress Analysis and Structural Strength Validation", Fraunhofer Institute for Structural Durability (LBF) ,Darmstadt;
retired Professor at the Faculty of Electrical Engineering, Mechanical Engineering and Naval Architecture (FESB), University of Split.
Zum Stetteritz 1, 64354 Reinheim, Georgenhausen, Germany

Jani Barle
Professor at the Faculty of Electrical Engineering, Mechanical Engineering and Naval Architecture (FESB), University of Split.
Ruđera Boškovića 32, 21000 Split, Croatia, (barle@fesb.hr)

UDK / UDC 577.3
Pregledni članak / Rewiev article
Prihvaćeno / Accepted: 19. 2. 2015.

THE POSITION OF THE IMPLANT FOR EXTRAARTICULAR FRACTURES OF THE DISTAL HUMERUS - THE NEW HYPOTHESES FOR MANAGEMENT

Srećko Sabalić, Janoš Kodvanj, Stjepan Jecić

Abstract

Through many stages of development, from conservative to operative treatment, open reduction and internal fixation with dual plating systems are the golden standard for fixation of distal humerus fractures. The plates are placed with a slight offset, posteromedially and posterolaterally. In recent publications, a higher stiffness and strength of osteosynthesis in the parallel plating technique were compared to the perpendicular technique with different plate designs. As noted in previous studies, non-union of the distal humerus usually occurs in the region at the metaphyseal and supracondylar level of radial columns due to varus stresses. Therefore the hypothesis is that in the case of extraarticular methphyseal fractures, which are treated with two plates perpendicular or parallel to form, the radial side of the plate should be longer than the ulnar side in order to prevent varus stresses as the main cause of the distal humeral pseudoarthrosis. Sufficient stability can be ensured with newly designed Y-shaped plate which should have a longer radial arm and be configured to prevent varus stresses. To prove this hypothesis, biomechanical studies at the supracondylar metaphyseal level on the border of the distal humerus diaphysis should be performed.

Keywords: distal humerus, extraarticular fracture, biomechanics

1. INTRODUCTION

Fractures of the distal humerus in adults are often challenging in operative treatment (1). In practice, it has been shown that 16% of humeral shaft and 10% of distal humerus fractures in adults are distal humeral shaft and extraarticular supracondylar humerus fractures (2).

The focus of this article is comminuted extraarticular distal humeral fracture. This type fracture often results from a gunshot wound (Figure 1) or motor vehicle

injuries in the younger population (2). Such injuries can also result from a simple fall in the elderly population (3).

A B

Figure 1. Gunshot fracture of the distal humerus treated with an external fixator (A) and later treated with osteosynthesis with two plates in the perpendicular position (90-90°) (B).

Slika 1 Prostrijelni prijelom distalnog humerusa liječen vanjskim fiksatorom (A) i osteosintezom s dvije pločice u perpendikularnoj konfiguraciji (90°-90°) (B)

The principal objective of treating extraarticular distal humeral fractures is restoring alignment and achieving stable fixation aimed at facilitating early elbow range of motion, essential for a good functional outcome. It is often difficult to obtain rigid fixation in distal fractures of the humeral diaphysis without compromising the elbow (4).

However, fixation of these fractures remains a challenge due to the restricted space for instrumentation at the distal segment and the need to maintain repair integrity under a large range of motion and low to moderate loading (5).

Through many stages of development, from conservative to operative treatment, open reduction and internal fixation with dual plating systems are the golden standard for fixation of distal humerus fractures (1,2,4,5,8-14). Double-plating techniques using two 3.5mm reconstruction plates or LCP plates in dorsal plating, 90-90 or 180-180 (Figure 2) pattern are generally accepted, for intra- (1,4,5,7-14,15-19) as well as extraarticular fractures (2,4,6,7). Previous studies have shown that surgery surpasses the results of conservative treatment (3,7). In the essence, the triple plating approach

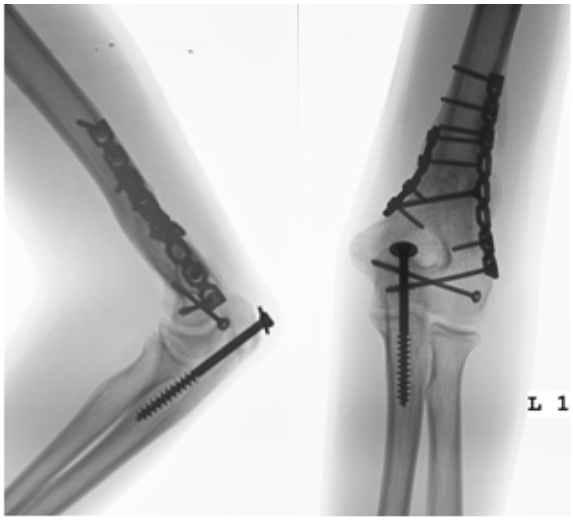

Figure 2. Double-plating techniques using two 3.5mm reconstruction plates in parallel (180-180°) pattern model

Slika 2. Osteosinteza s dvije rekonstrukcijske pločice 3,5 mm u paralelnom (180°-180°) položaju

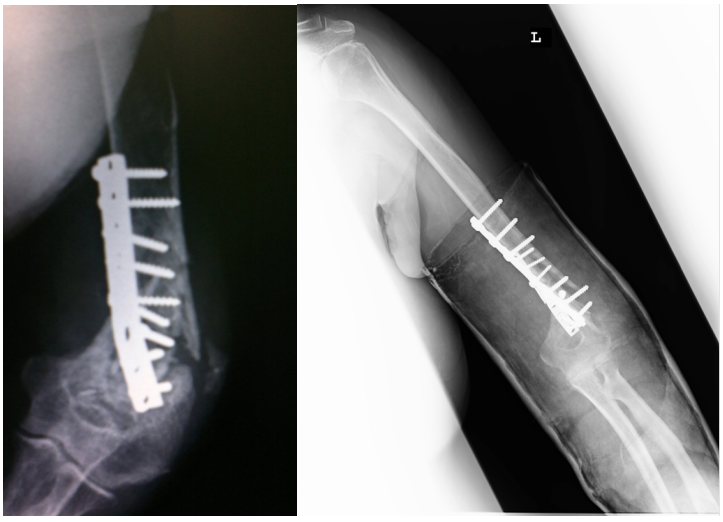

A B

Figure 3. Varus deformity after non-union of the extraarticular distal humeral fracture after osteosynthesis with one (A) and two (B) plate

Slika 3. Varusni deformitet kao posljedica nedostatnog cijeljenja ekstraartikularnog prijeloma distalnog humerusa nakon osteosinteze s jednom (A) i s dvije pločice (B)

is a combination of the above techniques. It is used in cases with severe comminution where additional fixation is required. Typically, the third plate is placed laterally to provide additional support for the radial column (20).

Even if the above mentioned techniques are applied this does not exclude a complication of distal humerus fractures, with a reported incidence of 20% to 25% (12). Poor initial fixation, which is not easily manageable in the presence of extensive comminution and osteopenia, can be the main factor for hardware failure (21).

Non-union with cubitus varus deformity (gunstock deformity) can occur when applied to inadequate osteosynthesis (Figure 3).

2. THE HYPOTHESES

Having applied the findings from previous biomechanical studies, as well as the results of clinical trials - particularly the complications in the form of pseudoarthrosis occurring in the postoperative period, and the findings relating to the ways of transferring the load to the distal humerus - we would like to present the following hypotheses:

1. In the case of extraarticular methphyseal fractures, which are treated with two plates (reconstruction or locking compression), perpendicular or parallel to form, the radial side of the plate should be longer than the ulnar side in order to prevent varus stresses as the main cause of the distal humeral pseudoarthrosis.

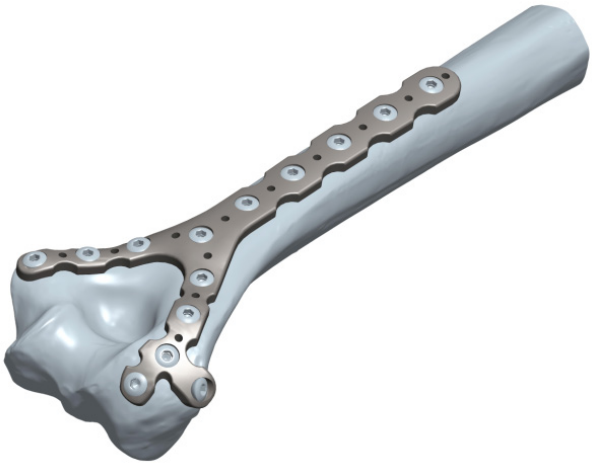

Figure 4. The new designed Y shaped plate should have a longer radial arm and should be configured to prevent varus stresses

Slika 4. Novodizajnirana Y pločica treba imati dulji radijalni krak i treba biti konfigurirana s ciljem izbjegavanja varusnih naprezanja

2. Sufficient stability can be ensured with new design Y-shaped reconstruction or Y-shaped locking compression plate. The Y shaped plate should have a longer radial arm and should also be configured to prevent varus stresses (Figure 4).
3. Parallel configuration is stronger than the perpendicular configuration on supracondylar metaphyseal level of the distal humerus under axial load in a position of flexion of 50^0 and in case of anterioposterior load in a position of flexion of 75^0 when the radial column carries 60% and 40% of the ulnar load. No significant difference in strength between the parallel and perpendicular configurations was observed on the radial condyle load.
4. The new design Y-shaped plate, as previously described, has a similar strength in the anterioposterior load, less strength in the axial load, and better strength in the lateral load to the radial condyle when compared with the parallel and perpendicular configuration. In addition, the plate is much stiffer in the anteroposterior and lateral load on the radial condyle and the lower axial load in comparison with the perpendicular configuration.

3. EVALUATION OF THE HYPOTHESES

The majority of non-unions happen at the supracondylar level, while healing of the articular components may occur in their reduced position. Nonetheless, the stability of the construct requires adequate bony contact with interfragmentary compression. In case of a distal humeral fracture, by far the greatest number of fixation failures occurs at the supracondylar level, while typically the articular fragments unite, and, with time, fracture union at this level.

Maximizing stability between the distal fragments and the shaft of the humerus at the metaphyseal level should be the focus of the fixation strategy (4,6). O'Driscoll (6) lists the technical principles to apply in order to achieve stable internal fixation of distal intraarticular humeral fractures.

Concerning the plates used for fixation, he writes that they should be applied in such a manner so as to achieve compression at the supracondylar level for both columns; at the same time the plates used must be strong enough and stiff enough to resist breaking or bending before union occurs at the supracondylar level (6).

The practical application of these principles involves "parallel" plates that permit a total of at least 4 to 6 long screws to be placed in the distal fragments, from one side across to the other. The plates are placed with a slight offset, posteromedially and posterolaterally (14).

Pajarinen et al (22) conclude that satisfactory results can be obtained when stability of the humeral columns is achieved and the articular platform reconstructed.

O'Driscoll (6) points out that the literature on fractures of the distal humerus pays far too little attention to how the failure of fixation generally begins in the lateral column. The force of gravity acting on the long lever arm (the forearm), while the elbow is flexed and extended during apparently minimal-use activities leads to repetitive varus stresses across the elbow. This can be typically seen in the action of a person reaching out to grab something, a glass of water for instance, followed by bringing the hand to the mouth. This causes varus torque across the elbow, distracting the lateral column away from the fixation placed along its posterior surface (6).

The load transfer in the elbow joint can be described by a two column model (1,23). The medial ulnar column and the lateral radial column form the articular block. The lateral column shares 60% of the load and the medial column 40% (1,18,23). This two-column model is the basic principle of the double plating osteosynthesis of C-type fractures of the distal humerus (1,6,12).

In recent publications, a higher stiffness and strength of osteosynthesis in the parallel plating technique were compared to the perpendicular technique with different plate designs. The mechanical advantages of a parallel plate configuration have been demonstrated for conventional reconstruction plate design (24), as well as for locking plate constructs (19). In other studies did not find a significant differences (1,5). As noted in previous studies, pseudoarthrosis of the distal humerus usually occurs in the region at the metaphyseal and supracondylar level of radial columns due to varus stresses.

So far, there have been no biomechanical studies on the supracondylar metaphyseal level on the border of the distal humerus diaphysis. Previous studies have examined intraarticular or low supracondylar fractures (16-19,24).

We believe that fractures in this part of the humerus have different biomechanical demands than intra-articular fractures of the distal humerus. The previously described new design Y shaped plate, which supports both columns and is at the same time longer in the radial, more loaded column, could be at least of the strength equal to the strength as the two plates.

To prove the hypotheses, the following tests should be performed: biomechanical studies at the supracondylar metaphyseal level on the border of the distal humerus diaphysis using the finite element method, where the gap would be done at the level of the distal humerus 3 cm above the fosse olecrani (Figure 5). The gap is shown in the figure as an interruption of the bone continuity.

The biomechanical study should be made to the axial load in a position of flexion of 5 , the bending load in a position of flexion of 75^0 and the lateral load on the radial condyle. After applying the finite element method in order to choose the optimal position of the plates, a biomechanical study of the synthetic or cadaver humerus would

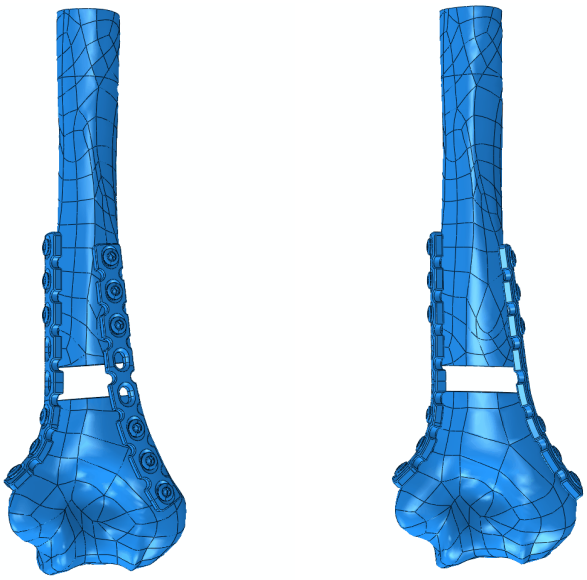

A B

Figure 5. Biomechanical model at the supracondylar humerus level of the distal humerus- perpendicular (A) and parallel configurations (B)

Slika 5. Biomehanički model suprakondilarnog dijela distalnog humerusa – perpendikularna (A) i paralelna konfiguracija (B)

be undertaken. This study would compare the stiffness of the new design Y-shaped parallel and perpendicular plate configuration by applying the same loads as those applied in the finite element method.

4. DISCUSSION

The incidence of distal humeral fracture is relatively small, with a large number of fracture subtypes. Clinical studies are often functionally insufficient because of the limited number of patients. There are no published prospective randomized studies, the majority of the studies were retrospective and carried out on a small number of samples. Therefore, on the basis of these clinical studies it is not possible to draw conclusions about the recommendable implant configuration in case of fractures of the distal humerus. A biomechanical study is therefore required.

In their publication, Penzkofer et al (1) state the following: "the system stiffness is influenced by two kinds of factors: factors which cannot be influenced by the sur-

geon and factors which allow the individual adjustment of an osteosynthesis. The initial situation is the fracture pattern and fracture geometry with the number and shape of the fragments. This initial fracture situation strongly dictates the options for plate positioning. On the other hand, the overall construct stability can largely be influenced by placing the plates at different anatomical positions". In their study they do not take into account the lateral load, as there is already a load in the position of flexion and extension.

Zalavras et al (19) found that parallel plate constructs had significantly higher stiffness than the perpendicular ones during cyclic varus loading. The measurement of displacement is not made precise measuring instruments at the gap. In this article loosening of the implants was defined as gross displacement (backing-out) of the screws during cyclic loading of the specimens. When done varus loading to failure resulted in ligamentous disruption in all specimens, which occurred prior to any catastrophic failure of fixation (19). In this way, they could't see a shift in the gap and assess the mechanical stability of the specimens.

Recent biomechanical studies, considered loads on the distal segment of the humerus in a position of flexion of 75^0 (18,19) or 50^0 (20) to the longitudinal axis of the humerus, or a position of flexion of 5^0 (19) or 15^0 (18). Only Zalavras et al (20) have performed radial varus loads.

In clinical studies, significantly better results were achieved with surgical rather than with conservative treatment of extra-articular distal humeral fracture (3,7). Shin et al (13) compared clinical outcomes in patients with intraarticular distal humerus fractures and concluded that both parallel and orthogonal plate positioning can provide adequate stability and anatomic reconstruction of the distal humerus fractures, while Sanchez-Sotelo et al (12, 14) preferred the parallel configuration.

Prasarn et al (4) recently reported their good clinical experience with the use of the locking compression plate for extraarticular fractures of the distal humerus, adding two additional reconstructive plates to the radial column.

As noted in previous studies, pseudarthrosis of the distal humerus usually occurs in the region at the metaphyseal and supracondylar level of the radial columns due to varus stresses.

Previous studies have been variously designed with different directions and types of loads, different static and dynamic forms and in different cycles and with very varied samples. Furthermore, measuring instruments and their degree of precision in measuring displacements and deformations are different and hardly comparable. Therefore, it is difficult to compare the results of biomechanical studies. Also, so far, displacements in different directions when loads are significantly different have

not been taken into account. Therefore, we believe that the direction of the load which causes greater displacements has a greater impact on the overall evaluation of the stability of the implant. Consequently, displacements in the bending and lateral loads to the radial condyle are considerably larger than the axial load, and thus with a greater significance in the overall assessment of the structural stability of implants. Therefore, the role of the implant is to neutralize the forces that cause the greater displacements in the area. Likewise, in the case of osteoporotic fractures, we should know that osteoporosis is more pronounced in the posteriolateral part of the radial condyle (25), and that the area of the lateral columns, especially the capitelum and the distal part of the lateral column, has very thin cortices (26).

After the biomechanical studies were conducted with the aim of proving or rejecting the hypothesis, randomized clinical medical trials should be performed. A disadvantage of biomechanical studies of this kind is the inability to take account of all factors that influence the treatment outcome. Dynamic loads that occur during everyday activities have important place among them.

Well known issue of anatomical variations in the distal humerus requires making plates of different size with the ability of remodeling regarding the anatomical differences.

The biomechanical study as described above can provide proof of the hypothesis that two plates where the plate at the radial side is longer or a new design Y-shaped plate as previously described provide improved biomehanical stability in comparison with two plates of equal length in fractures of distal humerus diaphysis at the turn of the distal humerus. The former method would prevent varus stresses and complications that arise due to this load.

5. CONFLICTS OF INTEREST STATEMENT

None declared.

Reference

[1] Penzkofer R, Hungerer S, Wipf F, von Oldenburg G, Augat P. Anatomical plate configuration affects mechanical performance in distal humerus fractures. Clin Biomech (Bristol, Avon) 2010;25(10):972-8.

[2] Tejwani NC, Murthy A, Park J, McLaurin TM, Egol KA, Kummer FJ. Fixation of extraarticular distal humerus fractures using one locking plate versus two reconstruction plates: a laboratory study. J Trauma 2009;66(3):795-9.

[3] Robinson CM, Hill RM, Jacobs N, Dall G, Court-Brown CM. Adult distal humeral metaphyseal fractures: epidemiology and results of treatment. J Orthop Trauma 2003;17(1):38-47.

[4] Prasarn ML, Ahn J, Paul O, Morris EM, Kalandiak SP, Helfet DL, Lorich DG. Dual plating for fractures of the distal third of the humeral shaft. J Orthop Trauma 2011;25(1):57-63.

[5] Schwartz A, Oka R, Odell T, Mahar A. Biomechanical comparison of two different periarticular plating systems for stabilization of complex distal humerus fractures. Clin Biomech 2006;21:950 –955.

[6] O'Driscoll SW. Optimizing stability in distal humeral fracture fixation. J Shoulder Elbow Surg 2005;14:186S-94.

[7] Jawa A, McCarty P, Doornberg J, Harris M, Ring D. Extra-Articular Distal-Third Diaphyseal Fractures of the Humerus. A Comparison of Functional Bracing and Plate Fixation. J Bone Joint Surg Am 2006 Nov;88(11):2343-7.

[8] Schatzker J., 2005. Fractures of the Distal End of the Humerus (13-A, B and C), in Schatzker J., Tile M., (Eds.), The Rationale of Operative Fracture Care. Springer, Berlin Heidelberg New York, 2005, pp: 103-121.

[9] McKee MD. Fractures of the shaft of the humerus. In Rockwood and Green's Fractures in Adults,Bucholz RW, Heckman JD, Court-Brown CM, Editors. Lippincott Williams & Wilkins: Philadelphia, 2006, pp:1117-1159.

[10] Becker EH, Stein J. Advancements in the Treatment of Distal Humeral Fractures. Current Orthopaedic Practice 2009;20(4):345–348.

[11] DeLuise A,Voloshin I. Current management of distal humerus fractures. Curr Opin Orthop 2006;(17):340–7.

[12] Sanchez-Sotelo J, Torchia ME, O'Driscoll SW. Complex distal humeral fractures: internal fixation with a principle-based parallel-plate technique. J Bone Joint Surg Am 2007;89:961-9.

[13] Shin SJ, Sohn HS, Do NH. A clinical comparison of two different double plating methods for intraarticular distal humerus fractures. J Shoulder Elbow Surg 2010;19(1):2-9.

[14] Sanchez-Sotelo J, Torchia ME, O'Driscoll SW. Principle-based internal fixation of distal humerus fractures. Tech Hand Up Extrem Surg 2001;5 (4): 179-87.

[15] Theivendran K, Duggan PJ, Deshmukh SC. Surgical treatment of complex distal humeral fractures: functional outcome after internal fixation using precontoured anatomic plates. J Shoulder Elbow Surg 2010;19(4):524-32.

[16] Korner J, Diederichs G, Arzdorf M, et al. A biomechanical evaluation of methods of distal humerus fracture fixation using locking compression plates versus conventional reconstruction plates. J Orthop Trauma 2004;18:286 –293.

[17] Schuster I, Korner J, Arzdorf M, Schwieger K, Diederichs G, Linke B: Mechanical comparison in cadaver specimens of three different 90 - degree double-plate osteosyntheses for simulated C2-type distal humerus fractures with varying bone densities. J Orthop Trauma 2008;22:113-120.

[18] Windolf M, Maza ER, Gueorguiev B, Braunstein V, Schwieger K. Treatment of distal humeral fractures using conventional implants. Biomechanical evaluation of a new implant configuration. BMC Musculoskelet Disord 2010;11:172.

[19] Zalavras CG, Vercillo MT, Jun BJ, Otarodifard K, Itamura JM, Lee TQ. Biomechanical evaluation of parallel versus orthogonal plate fixation of intra-articular distal humerus fractures. J Shoulder Elbow Surg 2011;20(1):12-20.

[20] Jupiter JB, Goodman LJ. The management of complex distal humerus nonunion in the elderly by elbow capsulectomy, triple plating, and ulnar nerve neurolysis. J Shoulder Elbow Surg 1992;1:37-55.

[21] Sommer C, Babst R, Müller M, Hanson B. Locking compression plate loosening and plate breakage: a report of four cases. J Orthop Trauma 2004;18(8):571-7.

[22] Pajarinen J, Bjorkenheim JM. Operative treatment of type C intercondylar fractures of the distal humerus: results after a mean follow-up of 2 years in a series of 18 patients. J Shoulder Elbow Surg 2002;11:48-52.

[23] Halls AA, Travill A. Transmission of pressures across the elbow joint. Anat Rec 1964.150, 243 – 247.

[24] Arnander MW, Reeves A, MacLeod IA, Pinto TM, Khaleel A. A biomechanical comparison of plate configuration in distal humerus fractures. J Orthop Trauma 2008;22(5):332-6.

[25] Park SH, Kim SJ, Park BC, Suh KJ, Lee JY, Park CW, Shin IH, Jeon IH. Three - dimensional osseous micro - architecture of the distal humerus: implications for internal fixation of osteoporotic fracture. J Shoulder Elbow Surg 2010;19(2):244-50.

[26] Diederichs G, Issever AS, Greiner S, Linke B, Korner J. Three-dimensional distribution of trabecular bone density and cortical thickness in the distal humerus. J Shoulder Elbow Surg 2009;18(3):399-407.

Položaj implantata kod ekstraartikularnih prijeloma distalnog humerusa – nove hipoteze za liječenje

Sažetak

U razvojnom procesu od konzervativnog pa do operativnog liječenja prijeloma distalnog humerusa, otvorena repozicija te unutrašnja fiksacija pločicama i vijcima su se pokazale kao najbolja metoda liječenja. Pločice se postavljaju uz blagi pomak posteromedijalno i posterolateralno. U posljednjim biomehaničkim studijama uglavnom je analizirana i uspoređivana krutost i stabilnost osteosinteze s različitim pločicama u paralelnoj i perpendikularnoj konfiguraciji. Dosadašnja istraživanja su također pokazala da su loši rezultati liječenja prijeloma distalnog humerusa uglavnom posljedica neadekvatnog cijeljenja u metafizarnoj i suprakondilarnoj regiji radijalne kolumne zbog varusnih naprezanja. Stoga je hipoteza rada da kod ekstraartikularnih metafizarnih prijeloma koji se liječe s dvije pločice u paralelnoj ili perpendikularnoj konfiguraciji, pločica na radijalnoj strani treba biti dulja od ulnarne kako bi se izbjegla varusna naprezanja koja su u većini slučajeva glavni uzročnik pojave pseudoartroze distalnog humerusa. Dovoljna stabilnost koštanih ulomaka može se osigurati novodizajniranom Y pločicom koja je konfigurirana na način da ima dulji radijalni krak, čime se znatno smanjuju varusna naprezanja. Da bi se navedena hipoteza dokazala, potrebno je provesti biomehanička istraživanja u suprakondilarnoj i metafizarnoj regiji na prijelazu u dijafizarnu regiju distalnog humerusa.

Ključne riječi: distalni humerus, ekstraartikularni prijelom, biomehanika

Srećko Sabalić, MD, PhD,
Trauma and General Surgeon, Clinical Hospital Center „Sisters of Mercy",
University Hospital for Traumatology Zagreb, Croatia. Corresponding Address: Medveščak 85, 10000 Zagreb
Phone:++38598514381. E-mail: ssabalic@gmail.com

Janoš Kodvanj, Professor, PhD, University of Zagreb,
Faculty of Mechanical Engineering and Naval Architecture, Ivana Lučića 5, Zagreb.
E-mail: janos.kodvanj@fsb.hr.
Award of the Croatian Academy of Sciences and Arts 2009.

Akademik Stjepan Jecić, Professor emeritus, PhD,
University of Zagreb, Faculty of Mechanical Engineering and Naval Architecture, Ivana Lučića 5, Zagreb.
E-mail: stjepan.jecic@fsb.hr.
Full member of the Croatian Academy of Sciences and Arts.

Rad 521. Technical sciences 17(2015)

Nakladnik / Publisher
HRVATSKA AKADEMIJA ZNANOSTI I UMJETNOSTI
Trg Nikole Šubića Zrinskog 11, 10000 Zagreb

Za nakladnika / For the Publisher
Akademik Pavao Rudan, glavni tajnik

Tehnički urednik / Graphical Editor
Ranko Muhek

Naklada / Copies
200

Tisak / Printed by
Intergrafika TTŽ, Zagreb

Zagreb, lipanj / june 2015.